NATIONAL ENERGY TECHNOLOGY LABORATORY

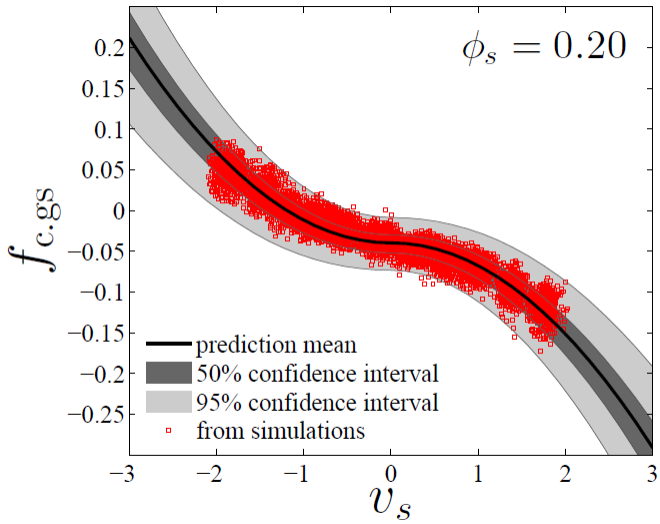

Annual Report: Carbon Capture Simulation Initiative (CCSI)

30 September 2013

NETL Technical Report Series

U.S. DEPARTMENT OF ENERGY

Office of Fossil Energy

NETL-TRS-CCSI-2013

Disclaimer

This report was prepared as an account of work sponsored by an agency of the United States Government. Neither the United States Government nor any agency thereof, nor any of their employees, makes any warranty, express or implied, or assumes any legal liability or responsibility for the accuracy, completeness, or usefulness of any information, apparatus, product, or process disclosed, or represents that its use would not infringe privately owned rights. Reference therein to any specific commercial product, process, or service by trade name, trademark, manufacturer, or otherwise does not necessarily constitute or imply its endorsement, recommendation, or favoring by the United States Government or any agency thereof. The views and opinions of authors expressed therein do not necessarily state or reflect those of the United States Government or any agency thereof.

Cover Illustration: The 50% and 95% confidence intervals in predicted filtered drag force based on uncertainty in β and γ.

Suggested Citation: David C. Miller, Madhava Syamlal, Roger Cottrell, Joel D. Kress, S. Sundaresan, Xin Sun, C. Storlie, D. Bhattacharyya, Charles Tong, Stephen E. Zitney, Crystal Dale, Dave Engel, Deb Agarwal, Paolo Calafiura, John Shinn, *Annual Report: Carbon Capture Simulation Initiative (CCSI),* NETL-TRS-CCSI-2013, NETL Technical Report Series, U.S. Department of Energy, National Energy Technology Laboratory, Pittsburgh, PA, 2013.

An electronic version of this report has been uploaded to the Office of Science, Technology, and Industry web site at: http://www.osti.gov/bridge/

Annual Report: Carbon Capture Simulation Initiative (CCSI)

Office of Research and Development, National Energy Technology Laboratory

NETL-TRS-CCSI-2013
30 September 2013

Contacts:
CCSI Technical Team Lead: David C. Miller, NETL
CCSI Technical Director: Madhava Syamlal, NETL
Project Coordinator: Roger Cottrell, URS/NETL

Basic Data Submodels and UQ Team
Lead: Joel D. Kress, LANL

High Resolution Filtered Submodels Team
Lead: S. Sundaresan, Princeton U.
Co-Lead: Xin Sun, PNNL

Validated High-fidelity CFD Models and UQ Team
Lead: Xin Sun, PNNL
Co-Lead: C. Storlie, LANL

Process Models Team
Lead: Prof. D. Bhattacharyya, WVU/NETL
Co-Lead: David C. Miller, NETL

Process Optimization and UQ Team
Lead: David C. Miller, NETL
Co-Lead: Charles Tong, LLNL

Integrated Framework for Dynamics and Control Team
Lead: Stephen E. Zitney, NETL

Risk Analysis & Decision Making Team
Lead: Crystal Dale, LANL
Co-Lead: Dave Engel, PNNL

Crosscutting Integration Tools Team
Lead: Deb Agarwal, LBNL
Co-Lead: Paolo Calafiura, LBNL

Industry Advisory Board
Coordinator: John Shinn, SynPatEco

Table of Contents

1.0 Executive Summary 1
2.0 Technical Highlights and Key Results 3
Scope of Project 3
Task 1: Project Management and Industry Advisory Board 4
Task 2.0 Basic Data Submodels and UQ 5
Task 3.0 High Resolution Filtered Submodels 9
Task 4.0 Validated High-fidelity CFD Models and UQ 15
Task 5.0 Process Models 22
Task 6.0 Process Optimization & UQ 30
Task 7.0 Integrated Framework for Dynamics & Control 34
Task 8.0 Risk Analysis & Decision Making 36
Task 9.0 Crosscutting Integration Tools 38
3.0 Conclusion 39
4.0 Technology Transfer 40
5.0 References 44

List of Figures

Figure 1: The 8 Product Categories of the CCSI Toolset 3

Figure 2: Calibration of the Simple Model with Discrepancy (Green Curves) to the "Reality" Function (Black Curve)..... 6

Figure 3: Temperature and Pressure Profiles for the Simple Model at the First Iteration. 6

Figure 4: Temperature and Pressure Profiles for the Simple Model at the Second Iteration..... 6

Figure 5: Comparison of Viscosity of 8 m 2MPZ and 8 m PZ. 8

Figure 6: Model Predictions of Liquid Film Mass Transfer Coefficient Compared to Experimental Data Measured on Pilot Scale Air-Water Column. Value of 1 on the Ordinate Indicates a Model Prediction Consistent with Experimental Measurements. 8

Figure 7: Simulation snapshot for average particle fraction of 0.40 (red=solids, blue= gas). 9

Figure 8: (a) Uncertainty in filtered drag model parameters β and γ, represented as a posterior probability distribution. (b) The 50% and 95% confidence intervals in predicted filtered drag force based on uncertainty in β and γ..... 10

Figure 9: Coarse-Grid Filtered Model Predictions vs. 'Exact' Solution (Red Lines) for (a) Solid Fraction and (b) Pressure Drop. Legends Denote the Ratio of Coarse Grid Size to Cylinder Spacing $\Delta_{\text{grid}}^{\text{coarse}} / a_{\text{cyl}}$ 10

Figure 10: (a) Temperature distribution around a heated tube at several resolutions, expressed in terms of particle diameter, d_p. (b) Numerical simulations of the local heat transfer coefficient (at a particular angular location) at different resolutions vs. the experimental data from Kim et al[1]..... 11

Figure 11: Temperature Profiles in the Heat Transfer Unit Cell..... 12

Figure 12: Predicted effects of particle size on the attrition propensity..... 13

Figure 13: Comparison of (a) the attrited mass loss (b) the particle velocity distribution between different jet cups..... 13

Figure 14: Elutriated Fines Due to Different Mechanisms with Jet Velocity of 100 m/s..... 14

Figure 15: Predicted Solid Fraction Contour of Post-Attrited Jet-Cup System by (a) E-L Based DEM Attrition Model (b) E-E based DQMOM Attrition Model..... 14

Figure 16: Illustration of Experiment Setup for AX and 32D Flow 15

Figure 17: Pressure Drop PDT3820 vs. Flow Rate..... 16

Figure 18: Pressure Drop PDT3820 vs. Flow Rate, with Different Particle Sizes..... 16

Figure 19: Pressure Drop PDT3820 vs. Flow Rate, with 7 UQ Parameters Including Particle Size..... 17

Figure 20: Validation of Steady-State Temperature in 32D Hot Non-Reacting Flow..... 18

Figure 21: Validation of Pressure Drop in 32D Cold Flow and Hot Non-Reacting Flow..... 18

Figure 22: Bed Temperature Below Coils, for First 15 Flow Conditions..... 19

Figure 23: Bed Temperature at Mid-Bed Location, for First 15 Flow Conditions. 19

Figure 24: Bed Temperature at Top Of Bed, for First 15 Flow Conditions. 20

Figure 25: Marginal Posterior Distributions of the Six Model Parameters for MFIX 21

Figure 26: BFB Model Configurations. 23

Figure 27: Gas Concentration Profile Plot for Underflow Type Configuration. 23

Figure 28: Temperature Profile Plot of Lower Stage Adsorber in 2-stage Underflow Type Configuration. 24

Figure 29: Dynamics of Overall CO_2 Capture for a Disturbance of 10% Step Change in Flue Gas Flowrate. 24

Figure 30: Temperature Profile Plot for Overflow Type Configuration. 25

Figure 31: Temperature Profile Plot of Lower Stage Regenerator in 2-stage Underflow Type Configuration. 25

Figure 32: Solids temperature profile in the regenerator 26

Figure 33: Molar loading of the ions in the regenerator 26

Figure 34: Comparison of solids temperature profiles in all the models 27

Figure 35: Transients in Solids Loading as a Result of a Ramp Increase in the Steam Flowrate to the Regenerator. 28

Figure 36: ACM Flowsheet of the Moving Bed Regenerator along with the Steam/BFW System. 28

Figure 37: Comparison of Different Surrogate Modeling Techniques 30

Figure 38 Simulation based optimization framework with heat integration 31

Figure 39: ASU Superstructure. 32

Figure 40: Comparison of GAMS and AspenPlus Results for Reboiler 2. 33

Figure 41: Eigenvalue Variation during the Transient Response of the Full and Reduced System. 35

Figure 42: Example Screen Shot from the Input System Worksheet of TRICCS. 37

Figure 43: Example Screen Shots from the Summary & Aggregation Worksheet of TRICCS. 37

List of Tables

Table 1: Contribution to Each Task by Lab 4

Table 2: Reaction set for 2MPZ. Dicarbamate 2 orders slower than for PZ. 7

Table 3: Diffusivity parameters for 2MPZ. 7

Table 4: Solids exit conditions from the bed 27

Table 5: Simulation Results, 1-CO_2 Removal Fraction, 2-Sorbent Loading 35

Acronyms, Abbreviations, and Symbols

Acronym	Descriptive Name
ACM	Aspen Custom Model/Modeler
ALAMO	Automated Learning of Algebraic Models for Optimization
AM	Activity Manager
AOD	Additive Output Disturbance
ARRA	American Recovery and Reinvestment Act of 2009
API	Application Programming Interface
BFB	Bubbling Fluidized Bed
BOD	Board of Directors
CCS	Carbon Capture and Storage
CCSI	Carbon Capture Simulation Initiative
CFD	Computational Fluid Dynamics
CMU	Carnegie Mellon University
CO2	Carbon Dioxide
DOE	Department of Energy
EFRC	University of California at Berkeley Energy Frontier Research Center
FAL	Focus Area Lead
FWP	Field Work Proposal
FY	Fiscal Year
IAB	Industry Advisory Board
ICP	Industrially-Relevant Challenge Problem
IEA	International Energy Agency
IPT	Integrated Project Team
LANL	Los Alamos National Laboratory
LBNL	Lawrence Berkeley National Laboratory
LLNL	Lawrence Livermore National Laboratory
MFIX	Multiphase Flow with Interphase eXchanges
MMPC	Multiple Model Predictive Control
MOF	Metal-Organic Framework
MPC	Model Predictive Control
MW	Megawatt Thermal
MWe	Megawatt Electric
MWh	Megawatt Hours
NETL	National Energy Technology Laboratory
ORD	Office of Research and Development
PC	Pulverized Coal

Acronym	Descriptive Name
PDE	Partial Differential Equation
Penn State or PSU	The Pennsylvania State University
PID	Proportional-Integral-Derivative
Pitt	University of Pittsburgh
PMP	Project Management Plan
PNNL	Pacific Northwest National Laboratory
RC	Release Candidate
R&D	Research and Development
ROM	Reduced Order Model
RSI	Random Step-Input
RUA	Regional University Alliance
SARS	Safety Analysis and Review System
SCC	Strategic Center for Coal
SOPO	Statement of Project Objectives
TC	Technical Coordinator
TLT	Technical Leadership Team
TM	Technology Manager
TMo	Technical Monitor
UQ	Uncertainty Quantification
URS	URS Corporation
VUQ	Validation and Uncertainty Quantification
WBS	Work Breakdown Structure
WVU	West Virginia University

1.0 Executive Summary

The Carbon Capture Simulation Initiative (CCSI) is a partnership among national laboratories, industry and academic institutions that is developing and deploying state-of-the-art computational modeling and simulation tools to accelerate the commercialization of carbon capture technologies from discovery to development, demonstration, and ultimately the widespread deployment to hundreds of power plants. The CCSI Toolset will provide end users in industry with a comprehensive, integrated suite of scientifically validated models, with uncertainty quantification (UQ), optimization, risk analysis and decision making capabilities. The CCSI Toolset incorporates commercial and open-source software currently in use by industry and is also developing new software tools as necessary to fill technology gaps identified during execution of the project. Ultimately, the CCSI Toolset will (1) enable promising concepts to be more quickly identified through rapid computational screening of devices and processes; (2) reduce the time to design and troubleshoot new devices and processes; (3) quantify the technical risk in taking technology from laboratory-scale to commercial-scale; and (4) stabilize deployment costs more quickly by replacing some of the physical operational tests with virtual power plant simulations.

CCSI is led by the National Energy Technology Laboratory (NETL) and leverages the Department of Energy (DOE) national laboratories' core strengths in modeling and simulation, bringing together the best capabilities at NETL, Los Alamos National Laboratory (LANL), Lawrence Berkeley National Laboratory (LBNL), Lawrence Livermore National Laboratory (LLNL), and Pacific Northwest National Laboratory (PNNL). The CCSI's industrial partners provide representation from the power generation industry, equipment manufacturers, technology providers and engineering and construction firms. The CCSI's academic participants (Carnegie Mellon University, Princeton University, West Virginia University, Boston University and the University of Texas at Austin) bring unparalleled expertise in multiphase flow reactors, combustion, process synthesis and optimization, planning and scheduling, and process control techniques for energy processes.

During Fiscal Year (FY) 13, CCSI announced the initial release of its first set of computational tools and models during the October 2012 meeting of its Industry Advisory Board. This initial release led to five companies licensing the CCSI Toolset under a Test and Evaluation Agreement this year.

By the end of FY13, the CCSI Technical Team had completed development of an updated suite of computational tools and models. The list below summarizes the new and enhanced toolset components that were released following comprehensive testing during October 2013.

1. FOQUS. Framework for Optimization and Quantification of Uncertainty and Sensitivity. Package includes: FOQUS Graphic User Interface (GUI), simulation-based optimization engine, Turbine Client, and heat integration capabilities. There is also an updated simulation interface and new configuration GUI for connecting Aspen Plus or Aspen Custom Modeler (ACM) simulations to FOQUS and the Turbine Science Gateway.
2. A new MFIX-based Computational Fluid Dynamics (CFD) model to predict particle attrition.
3. A new dynamic reduced model (RM) builder, which generates computationally efficient RMs of the behavior of a dynamic system.
4. A completely re-written version of the algebraic surrogate model builder for optimization (ALAMO). The new version is several orders of magnitude faster than the initial release and eliminates the MATLAB dependency.
5. A new suite of high resolution filtered models for the hydrodynamics associated with horizontal cylindrical objects in a flow path.
6. The new Turbine Science Gateway (Cluster), which supports FOQUS for running multiple simulations for optimization or UQ using a local computer or cluster.
7. A new statistical tool (BSS-ANOVA-UQ) for calibration and validation of CFD models.

8. A new basic data submodel in Aspen Plus format for a representative high viscosity capture solvent, 2-MPZ system.
9. An updated RM tool for CFD (REVEAL) that can create a RM from MFIX. A new lightweight, stand-alone version will be available in late 2013.
10. An updated RM integration tool to convert the RM from REVEAL into a CAPE-OPEN or ACM model for use in a process simulator.
11. An updated suite of unified steady-state and dynamic process models for solid sorbent carbon capture included bubbling fluidized bed and moving bed reactors.
12. An updated and unified set of compressor models including steady-state design point model and dynamic model with surge detection.
13. A new framework for the synthesis and optimization of coal oxycombustion power plants using advanced optimization algorithms. This release focuses on modeling and optimization of a cryogenic air separation unit (ASU).
14. A new technical risk model in spreadsheet format.
15. An updated version of the sorbent kinetic/equilibrium model for parameter estimation for the 1st generation sorbent model.
16. An updated process synthesis superstructure model to determine optimal process configurations utilizing surrogate models from ALAMO for adsorption and regeneration in a solid sorbent process.
17. Validation models for NETL Carbon Capture Unit utilizing sorbent AX. Additional validation models will be available for sorbent 32D in 2014.
18. An updated hollow fiber membrane model and system example for carbon capture.
19. An updated reference power plant model in Thermoflex that includes additional steam extraction and reinjection points to enable heat integration module.
20. An updated financial risk model in spreadsheet format.

2.0 Technical Highlights and Key Results

Figure 1 shows the 8 major product categories (Tasks) of the CCSI Toolset. These categories correspond with the activities involved with the development of a new chemical process, such as a carbon capture system. This includes the development of submodels for basic data, such as thermodynamics and kinetics, and using those submodels within process models to synthesize and optimize a process design. The next major activity is identifying promising device configurations to serve as the basis for more detailed CFD simulations, then pulling all the information together to assess project risk and determine whether or how to proceed. Unique within CCSI is the integration of uncertainty quantification among the simulation scales. To effectively design a new process with new technology, each of these blocks is important and must interact to achieve an efficient, cost effective system.

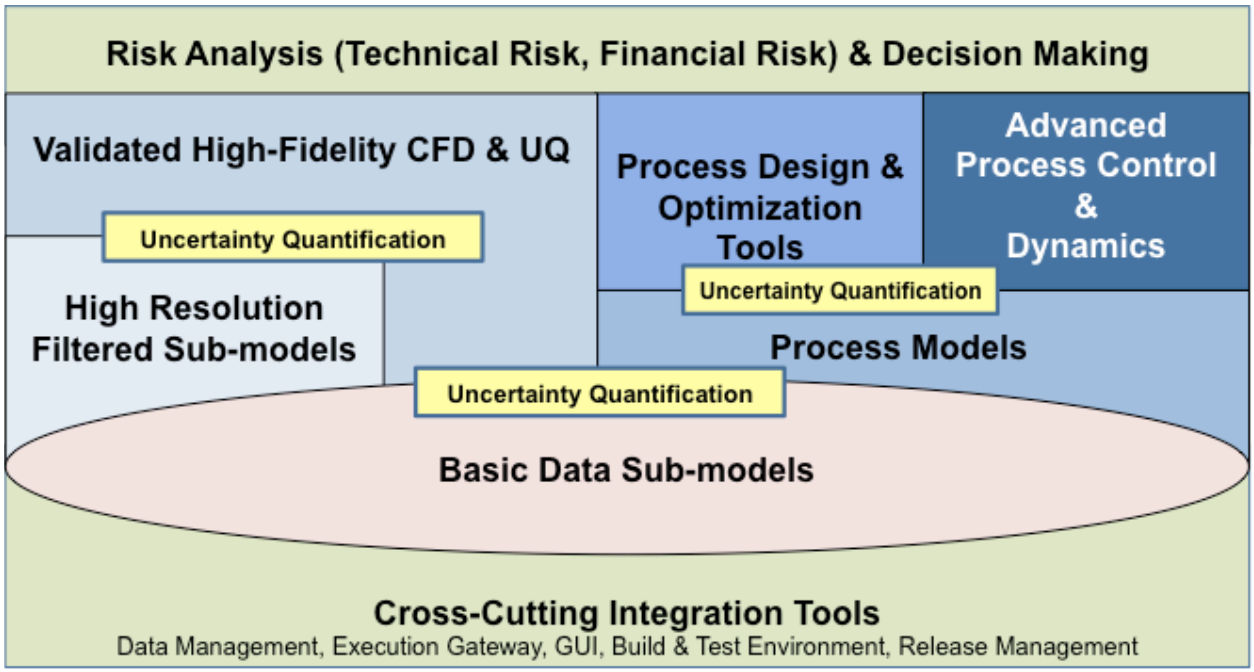

Figure 1: The 8 Product Categories of the CCSI Toolset

Scope of Project

Solid-sorbent-based post-combustion capture technology served as the initial demonstration technology for CCSI. Beginning with this project year, we will begin to wrap up the development of solid sorbent specific models and expand the demonstration capture technology to solvent systems. The project's task structure is organized around the 8 product categories: basic data submodels, high resolution filtered submodels, validated high-fidelity CFD models & UQ, steady-state and dynamic process models, process optimization & UQ, integrated framework for dynamics & control, risk analysis & decision making, and crosscutting integration tools, each as a major technical task in addition to Project Management (Task 1). The work in this project represents the combined work across five national labs and five universities. Table 1 shows the contribution, by lab, to each Task in this project.

Table 1: Contribution to Each Task by Lab

Task	NETL	LANL	LBNL	LLNL	PNNL
1: Project management	Lead				
2: Basic data submodels		Lead			
3: High resolution filtered submodels	Lead				Co-Lead
4: Validated high-fidelity CFD models & UQ		Co-Lead			Lead
5: Process Models	Lead				
6: Process optimization & UQ	Lead			Co-Lead	
7: Integrated framework for dynamics & control	Lead				
8: Risk analysis & decision making		Lead			Co-Lead
9: Crosscutting integration tools			Lead		

Task 1: Project Management and Industry Advisory Board

The technical team updated its Year 3 activities and developed a new organizational structure. This new organizational structure responds to feedback from its Industry Advisory Board (IAB) and DOE Headquarters (HQ). In addition, it incorporates new opportunities that were identified during the initial two years of the project (February 2011 through January 2012 under American Recovery and Reinvestment Act of 2009 (ARRA) funding and February 2012 through January 2013 under Advanced Research funding). The new features of CCSI that were initiated this year include (1) the launch of modeling activities related to solvent based CO_2 capture, (2) the integration of UQ activities coupled directly with three types of modeling activities, and (3) the introduction of a new approach for developing and applying dynamic process simulation.

Industry Advisory Board (IAB). Two meetings of the IAB were conducted. The first in October 2012 focused on the initial release of the CCSI Toolset. The second, in April 2013, introduced the new CCSI organizational structure and new solvent component of the program.

In October 2012, the CCSI Technical Team met with representatives from the 19 companies currently participating in its IAB to present its first set of computational tools and models. This pre-release, a year ahead of the originally planned first release, was the result of intense industry interest in getting early access to the tools and the rapid progress of the CCSI technical team. These initial components of the CCSI Toolset provided new models and computational capabilities that will accelerate the commercial development of carbon capture technologies and a broad range of technology development in general (power, refining, chemicals production, gas production, etc.). Following the industry advisory board workshop, Dr. John Shinn, the CCSI IAB coordinator, reported that “IAB members found the program progress impressive, well beyond what they might have expected at this point in the program, and that the program continues to be very well coordinated...the CCSI tool set pre-release of 21 technology deployment support tools, which appeared well ahead of original schedule, was very well received by the member companies with multiple members making immediate plans for adoption of the tools. The toolset is seen as being highly applicable for the CCSI core objectives (accelerating carbon capture deployment) as well as a broad range of other industry technology development and deployment applications.”

In April 2013, the CCSI Technical Team conducted its bi-annual program review meeting to highlight continued progress on the development of the CCSI Toolset, preview new capabilities that will be available in the next release, and assist companies seeking to adopt tools to accelerate their own

development projects. Several companies sent large contingents to this meeting, including potential users of the tools, in addition to senior management.

Following the April IAB meeting, two companies invited a subset of the CCSI Technical Team to visit their R&D centers to discuss capabilities of the CCSI Toolset and pave the way for them to license the tools, to introduce the capabilities of the tools to a broader cross section of its personnel, and also to explore ways they could collaborate more closely with the CCSI team. A visit was also made to the National Carbon Capture Center to discuss validation data for solvent systems, which is a new priority within CCSI. In several discussions with the CCSI Technical Team, one company has indicated that they have dedicated resources to utilize several components of the CCSI Toolset within their organization over the next 18 months. A CRADA with another has been finalized, which will provide CCSI access to detailed larger scale validation data and provide an opportunity for the toolset to be used to help scale up and further develop the process.

Task 2.0 Basic Data Submodels and UQ

Task 2 continued the development of submodels for solid sorbent carbon capture materials and initiated efforts in the development of appropriate submodels for solvent-based carbon capture as well. Major accomplishments related to solid sorbents include the development of an approach to statistically account for model discrepancy and incorporate it into process models. The accomplishments related to solvents include the development of a benchmark MEA model and the development of a submodel for a representative high viscosity solvent (2-MPZ).

<u>Solid sorbent model development</u>: Development focused on incorporating model discrepancy into the 1st generation lumped kinetic model with ideal, 1st-order kinetics:

$$\begin{aligned} 2R_2NH + CO_2(gas) &\rightleftharpoons R_2NCO_2^- + R_2NH_2^+ \\ R_2NH + H_2O(phys) + CO_2(gas) &\rightleftharpoons HCO_3^- + R_2NH_2^+ \\ H_2O(gas) &\rightleftharpoons H_2O(phys) \end{aligned}$$

The discrepancy is an advanced uncertainty quantification approach that will enable the submodel to be used more effectively for process scale up. A rate-based discrepancy solver was implemented and tested on a simple test problem. The test problem consisted of a very simple version of the 1st gen model, with a simulated “reality” that was effectively a two-step chemical rate expression. The model for this “reality” was then a single-step rate expression plus a Bayesian Smoothing Spline-Analysis of Variance (BSS-ANOVA) discrepancy term.

Following this initial demonstration, chemical models with discrepancy have been incorporated into process models of a bubbling fluidized bed adsorber. These efforts are ongoing, but have shown significant progress on two fronts: (1) a hypothetical simple model used to test the discrepancy modeling and iteration concepts, and (2) the full first-generation sorbent model.

In the simple model case, the two-step “reality” function (corresponding to a two-step adsorption process involving equilibrated formation of a zwitterion intermediate) was used to generate an initial set of hypothetical TGA data. A simpler, one-step model (direct formation of carbamate from the gas) plus discrepancy was then calibrated to this model, yielding a set of plausible model functions that reproduce the data to a reasonable extent (see Figure 2).

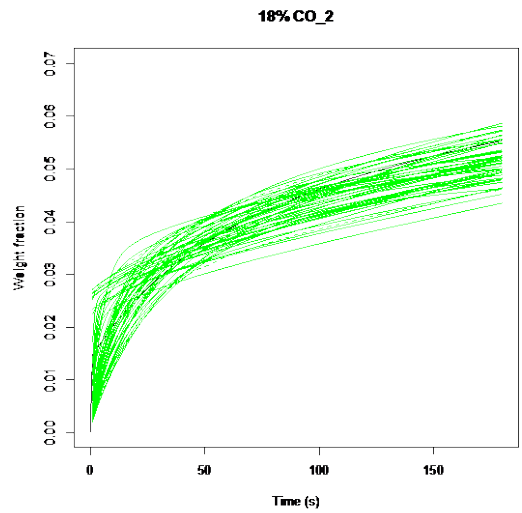

Figure 2: Calibration of the Simple Model with Discrepancy (Green Curves) to the "Reality" Function (Black Curve).

These functions were then incorporated into the bubbling fluidized bed model, yielding a set of curves that diverged widely as shown in Figure 3. These pressure and temperature profiles were then used to produce a second set of hypothetical TGA data by applying the "reality" function to a number of temperature and pressure profiles. As shown in Figure 4, the resulting profiles converge. Additional work is ongoing to reconcile inconsistencies in the converged model with discrepancy and the reality function.

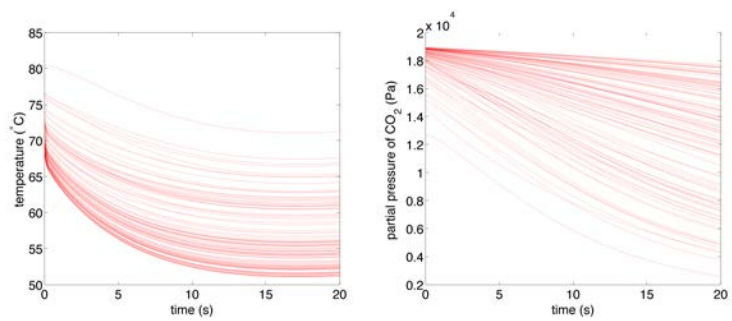

Figure 3: Temperature and Pressure Profiles for the Simple Model at the First Iteration.

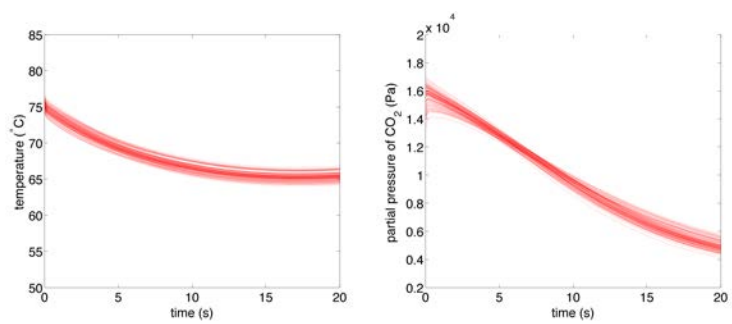

Figure 4: Temperature and Pressure Profiles for the Simple Model at the Second Iteration.

MEA solvent model for benchmarking: Basic data submodels for a number of physical properties in the MEA solvent model were updated and re-calibrated with experimental data. This updated and validated model will ultimately be incorporated into a benchmark MEA process model, which will be validated against pilot scale data from the National Carbon Capture Center (NCCC). The specific physical property submodels for which updated parameters have been determined include viscosity, density, and surface tension. Each of these physical properties strongly affects other models, which are used to calculate the rate at which CO_2 is absorbed.

High viscosity solvent model: A thermodynamic and kinetic model for the high viscosity CO_2 capture solvent, 2-MPZ was developed. This model will serve as a framework for future high viscosity solvent-based capture systems. Currently, accurate models for such carbon capture solvents do not exist, but they are of interest to industry since many new classes of potential carbon capture solvents have higher viscosities.

The thermodynamic model is based off the work of Chen (2011). The kinetics were regressed using a wetted wall column (WWC) Aspen Plus® simulation to adjust reaction rate constants, activation energies, and diffusion parameters to match experimental flux values within 20% (Plaza, 2011). The complete reaction set used is shown in Table 2.

Table 2: Reaction set for 2MPZ. Dicarbamate 2 orders slower than for PZ.

Reaction	k_o (kmol/s-m^3)	E_A (kJ/mol)
$2MPZCOO^- + H_2O + CO_2 \rightarrow H2MPZCOO + HCO_3^-$	2.62E6	98.0
$2\ 2MPZ + CO_2 \rightarrow 2MPZH^+ + 2MPZCOO^-$	1.45E10	21.9
$2\ 2MPZCOO^- + CO_2 \rightarrow 2MPZ(COO^-)_2 + H2MPZCOO$	1.28E10	21.9
$H2MPZCOO + HCO_3^- \rightarrow 2MPZCOO^- + H_2O + CO_2$	3.67E5	174
$2MPZH^+ + 2MPZCOO \rightarrow 2\ 2MPZ + CO_2$	3.96E4	97.8
$2MPZ(COO^-)_2 + H2MPZCOO \rightarrow 2\ 2MPZCOO^- + CO_2$	2.71E8	129

The diffusivity parameters of Equation 3 were also regressed.

$$D = D_o \left(\frac{T}{T_{ref}} \right)^{\beta} \left(\frac{\mu}{0.0465} \right)^{\alpha} \tag{3}$$

Table 3: Diffusivity parameters for 2MPZ.

Diffusivity Parameter	8 m 2MPZ value
D_o	4.4E-11 m^2/s
α	-1.50
β	-11.5
T_{ref}	373.15 K

In order to isolate the effect of steric hindrance in 2MPZ from the effect of viscosity, the viscosity subroutine for 2MPZ was replaced with that of PZ. The set of WWC experimental data for 8 m 2MPZ was used as a basis for comparison of 8 m PZ and 8 m 2MPZ. This removes the confounding variable of viscosity, leaving the effect of steric hindrance. A comparison of the viscosity of the two systems is shown in Figure 5. With both systems having the same viscosity, the remaining kinetic differences are attributable to steric hindrance. Steric hindrance has the largest impact at high loading and low temperature. At low temperature, the rate of reaction is more controlling than at high temperature, so the slowing effect of steric hindrance is more pronounced. Similarly, at high loading most of the unhindered amine group has been made into carbamate and so the decreased stability of the dicarbamate results in lower rates.

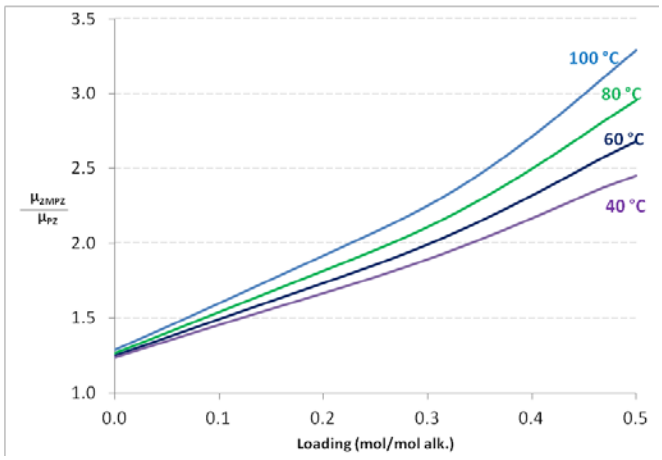

Figure 5: Comparison of Viscosity of 8 m 2MPZ and 8 m PZ.

Finally, empirical mass transfer models were developed using data collected at the Separations Research Program (SRP) at the University of Texas at Austin. The results of the regression for the Liquid-Side Mass Transfer Coefficient (k_L) are summarized in Figure 6. All regressed parameters (A, x1, x2) were statistically significant within their 95% confidence intervals.

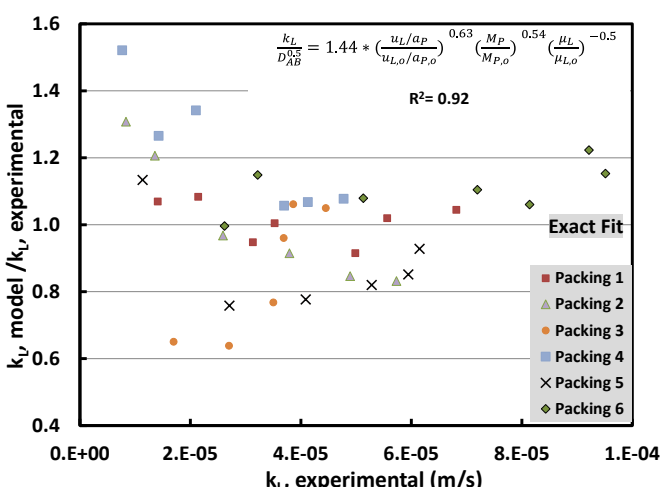

Figure 6: Model Predictions of Liquid Film Mass Transfer Coefficient Compared to Experimental Data Measured on Pilot Scale Air-Water Column. Value of 1 on the Ordinate Indicates a Model Prediction Consistent with Experimental Measurements.

Task 3.0 High Resolution Filtered Submodels

The major activities in this task involve the development of detailed models to support more detailed and accurate device scale modeling. Three types of models are under development: (1) filtered particle models, (2) filtered solvent models, and (3) a model of particle attrition. Accomplishments for each area are described below.

Filtered Particle Models: The particle submodels developed this year focus on hydrodynamic models for heat transfer tubes and related heat transfer models that are a function of particle size, and hydrodynamics. Gas-particle flow simulations (using MFIX) were performed in 2D periodic cells with horizontal immersed cylinder arrays for several different cylinder diameters, cylinder spacings, gas/particle velocities, and particle fractions as shown in Figure 7. The simulation results were then analyzed to derive filtered models for sub-grid drag. A complete 2D model for the sub-grid drag is now available.

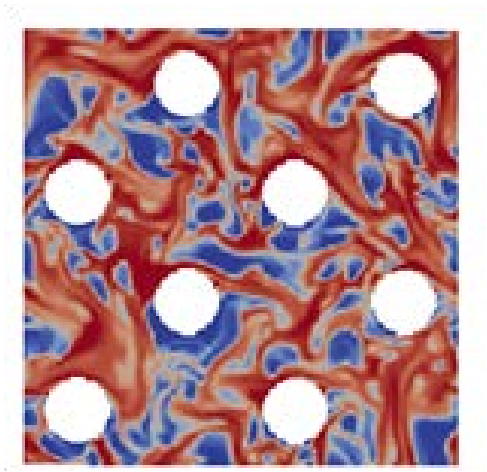

Figure 7: Simulation snapshot for average particle fraction of 0.40 (red=solids, blue= gas).

Model parameters for the hydrodynamic filtered models were computed using inherently fluctuating velocities and forces. Therefore, they have associated uncertainties, which must be quantified. A Bayesian UQ analysis was developed to compute the uncertainty associated with the filtered drag models, represented as a joint probability plot of the principal parameters β and γ (which appear in the filtered drag model[3]) in Figure 8(a). The uncertainty in the model parameters lead to an uncertainty in the predicted filtered drag force for given flow conditions. The 50% and 95% confidence intervals of the filtered drag force predictions are shown in Figure 8(b). The model uncertainty is quantified for varying velocity, solid fraction, and cylinder configuration.

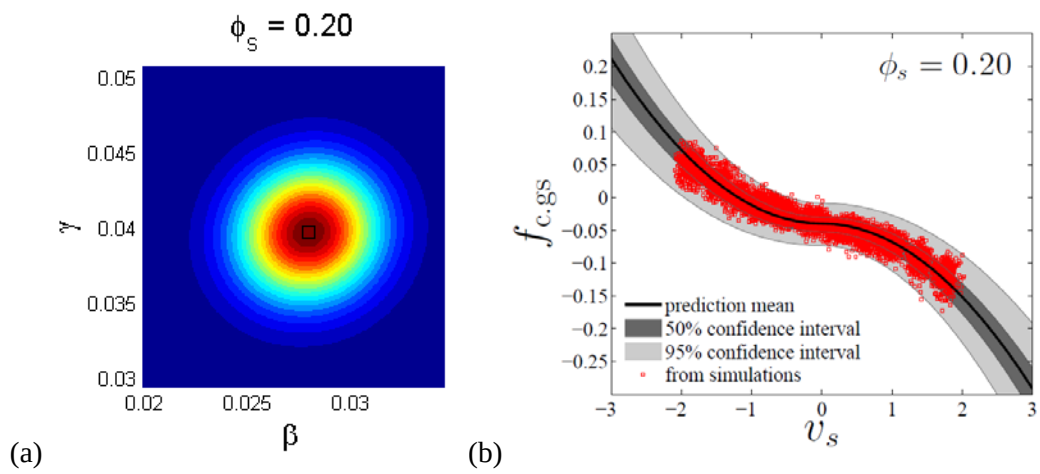

Figure 8: (a) Uncertainty in filtered drag model parameters β and γ, represented as a posterior probability distribution. (b) The 50% and 95% confidence intervals in predicted filtered drag force based on uncertainty in β and γ.

Coarse-grid predictions obtained using the filtered drag models were compared against a highly-resolved simulation, treated as the 'exact' solution, of a medium-sized (0.9 m × 1.8 m) turbulent fluidized bed. Comparisons of the sorbents solid fraction distribution and pressure drop with height from coarse-grid simulations show good agreement with the 'exact' solution in the lower regions of the bed (Figure 9). However, oscillations in the solid fraction above and below each row of tubes, observed in the 'exact' solution, were not resolved in the coarse-grid simulations (as expected) as the grid sizes are large compared to the tube diameter (Dcyl) and spacing (acyl). The filter size (i.e., the coarse-grid length) was found to have little influence on the predicted bed solid fraction.

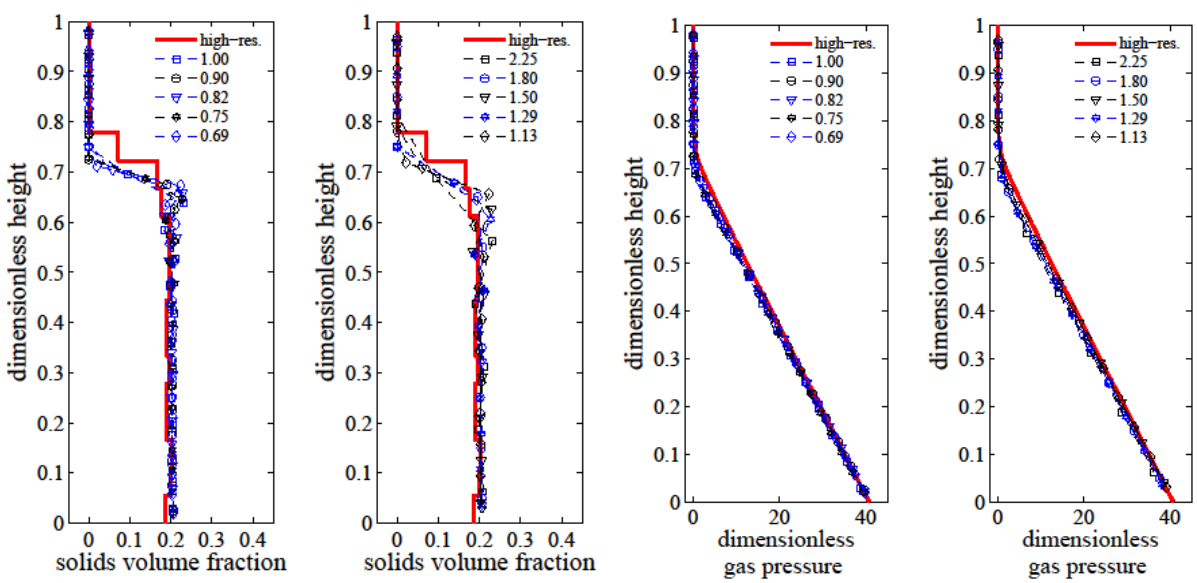

(a) **(b)** **(c)** **(d)**

Figure 9: Coarse-Grid Filtered Model Predictions vs. 'Exact' Solution (Red Lines) for (a) Solid Fraction and (b) Pressure Drop. Legends Denote the Ratio of Coarse Grid Size to Cylinder Spacing $\Delta_{\text{grid}}^{\text{coarse}} / a_{\text{cyl}}$.

Preliminary results (Figure 10) show the effects of resolution on global heat transfer predictions such as overall heat transfer coefficient and temperature distribution.

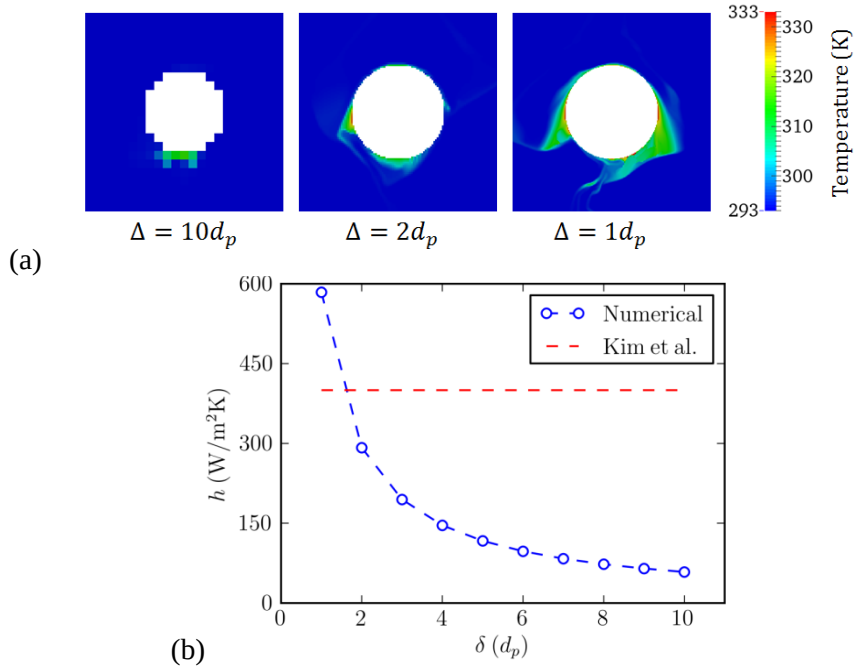

Figure 10: (a) Temperature distribution around a heated tube at several resolutions, expressed in terms of particle diameter, d_p. (b) Numerical simulations of the local heat transfer coefficient (at a particular angular location) at different resolutions vs. the experimental data from Kim et al[1].

In addition, a periodic unit cell consisting of two heat transfer tubes has been setup (Figure 11) and research has focused on appropriate boundary conditions for the unit cell. Setting up the heat transfer unit cell is more complicated than a pure hydrodynamics unit cell due to the variation in temperatures throughout the cell. With hydrodynamics, the overall mixture momentum is conserved and a statistically steady velocity field will develop in the unit cell. In heat transfer calculations, however, a hot two-phase flow enters along the bottom boundary of the cell and is cooled by the heat transfer tubes. If purely periodic conditions were applied in the flow direction the unit cell would eventually reach thermal equilibrium with the two-phase flow at the cool temperature of the heat transfer tubes. To avoid this scenario, boundary conditions must be applied to the cell to mimic a hot flow coming in.

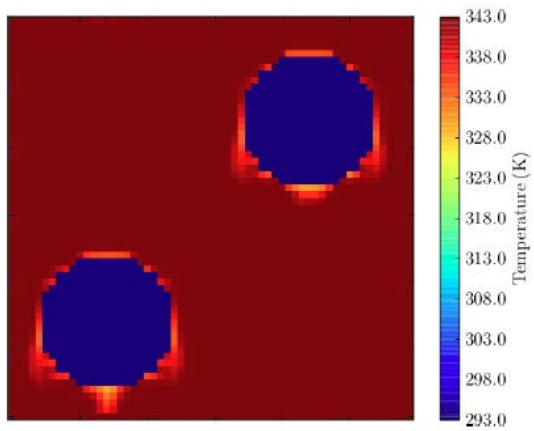

Figure 11: Temperature Profiles in the Heat Transfer Unit Cell.

The filtered heat transfer model research has also investigated appropriate modifications to the energy conservation equations. The "detailed" energy conservation equation is solved for both the gas (g) and solids (s) phase using the basic conservation equation with the addition of an interphase heat transfer term (Hgs), and the heat transfer tubes appear as boundary conditions. In the filtered model, the heat gained from the heat transfer tubes will appear as volumetric sources (Hgc, Hsc); further, the effective rate of heat exchange between the gas and particles in the bed will be modified to represent an "average" over the filtering space. These modifications will result in the following energy conservation equations,

$$\begin{aligned}
\phi_g \rho_g C_{p,g} \left(\frac{\partial T_g}{\partial t} + \boldsymbol{u}_g \cdot \nabla T_g \right) &= -\nabla \cdot \boldsymbol{q}_g - H_{gs} + H_{gc} \\
\phi_s \rho_s C_{p,s} \left(\frac{\partial T_s}{\partial t} + \boldsymbol{u}_s \cdot \nabla T_s \right) &= -\nabla \cdot \boldsymbol{q}_s + H_{gs} + H_{sc}
\end{aligned} \tag{2}$$

<u>Filtered Models for Solvent Systems</u>: A detailed literature review on CFD modeling of solvent absorption revealed a lack of fundamental large-scale CFD model studies for solvent absorption. The closest related literature concerned trickle bed applications and the associated CFD models employ primitive closures. A few publications present multi-scale approaches for solvent modeling, but these resulted in either large-scale mechanistic models with limited flexibility or large-scale pseudo-single phase CFD models that may be inappropriate for modeling the fully reactive two-phase flow system.

Based on techniques published in the literature, an approach was formulated to develop a large-scale CFD model with improved sub-model closures. The approach consists of two parallel CFD activities: 1) simulations based on an Eulerian-Eulerian (E-E) model implemented in MFIX where the packing is to be treated as porous medium and using available closure models, and 2) simulations based on a Volume-of Fluid (VOF) approach to two-phase flow through a representative packing geometry. The former can be used to conduct exploratory simulations to better understand the types of flow and absorption behavior that are predicted and to give insights on the relative importance of various terms. The purpose of the latter is to deduce more accurate closure models (for example, the interfacial interaction forces) for the former. Development of these detailed submodels for both packing/solvent interaction and for solvent/gas distribution in a large scale solvent-based capture system will be useful for both CFD device-scale simulations and process models.

Attrition Model: The attrition model will enable the prediction and tracking of changing particle size within device-scale CFD simulations. Two technical approaches, a discrete element method and an Eulerian-Eulerian method, have been adopted. The first describes the gas flow in the Eulerian system but explicitly resolves the motion of particles in the Lagrangian framework, while the latter considers both phases through the Eulerian approach. Using the first method, particulate attrition within a jet cup has been numerically studied. The predicted effects of particle size on the attrition propensity are shown in Figure 12, where monodispersed particles with diameters equal to 0.02, 0.03, 0.05, and 0.06 cm at the jet velocity of 150 m/s were simulated.

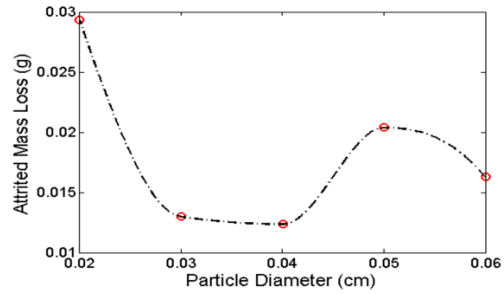

Figure 12: Predicted effects of particle size on the attrition propensity

The dependence appears to be rather nonlinear, which might result from combining effects of two counteracting mechanisms underpinning the attrition process: larger particle size reduces the fluidization but increases the external surface area and amplifies the colliding chance. For substantially smaller particles, the ones with diameter between 0.02-0.04 cm in the current work, attrition primarily relies on the velocity of the particles mobilized by the air jet. However, when particles become comparatively large, the collision rate becomes dominant. Further increases in the particle size causes the influence of limited carrying capacity of the air jet to gradually prevail and starts to hinder the attrition process.

It has also been found that the resistance to particulate attrition depends on the design of the testing apparatus. Figure 13(a) shows that compared to the baseline rectangular jet cup, a trapezoidal cup tends to yield lower attrited mass loss, which is primarily due to the more stagnant bed materials in the flow field as indicated in Figure 13(b).

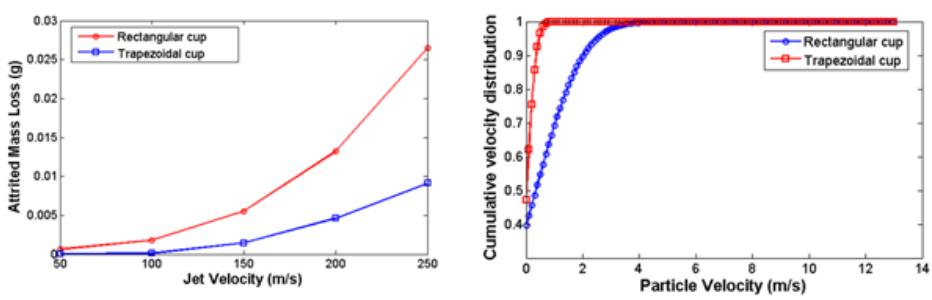

(a) (b)

Figure 13: Comparison of (a) the attrited mass loss
(b) the particle velocity distribution between different jet cups

Additionally, in order to address the respective contributions of particle-wall and particle-particle interactions to the generation of fines, the DEM model has been extended to analyze these sources of particulate attrition. Figure 14 shows an example of the elutriation attributed to different mechanisms in volume percentages. It can be seen that impact induced erosive chipping is clearly the dominant

mechanism over the abrasive mechanism, and the influence of particle-wall and particle-particle interactions of the chipping mechanism appears to be slightly biased toward particle-wall collisions.

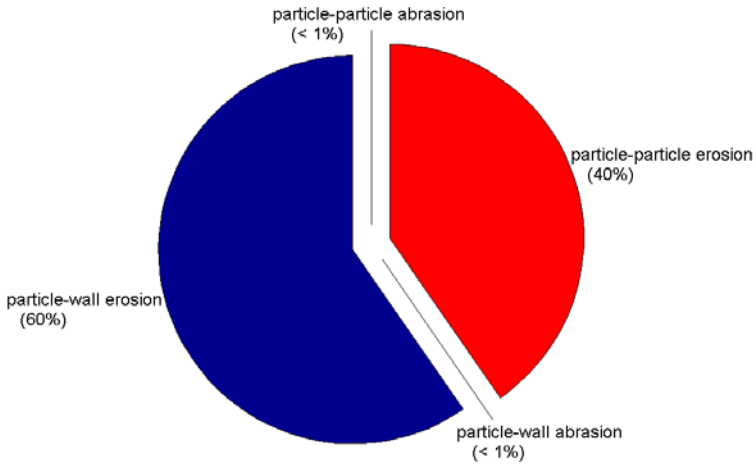

Figure 14: Elutriated Fines Due to Different Mechanisms with Jet Velocity of 100 m/s

In addition, we implemented a new attrition module in the direct quadrature method of moments (DQMOM) population balance model. This incorporates the mechanistic fragmentation capabilities of the previous discrete element model (DEM) into the E-E framework of MFIX. The DQMOM based attrition module has been successfully implemented in both serial and parallel versions of MFIX and is currently being calibrated and verified against the DEM model as shown in Figure 15. Compared to the Eulerian-Lagrangian (E-L) coupled DEM model, the current E-E based DQMOM model has a significant increase in computational efficiency: using 16 processors it takes less than ½ hour to complete 1-second simulation, compared to the 1.5 days needed by the DEM model. Therefore, the DQMOM model is particularly useful for large-scale system simulations with chemical reactions involved.

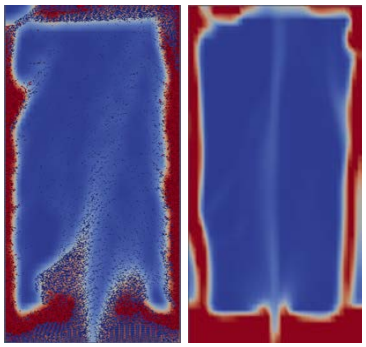

(a) **(b)**

Figure 15: Predicted Solid Fraction Contour of Post-Attrited Jet-Cup System by (a) E-L Based DEM Attrition Model (b) E-E based DQMOM Attrition Model.

Task 4.0 Validated High-fidelity CFD Models and UQ

The emphasis of this task is the development of high-fidelity CFD models and the UQ tools to enable their calibration and validation. We employ a hierarchical validation process according to the CCSI validation plan by validating and calibrating the different modules of the CFD models for the overall reactive multi-phase simulations into including hydrodynamics, coupled hydrodynamics and heat transfer, and coupled hydrodynamics, heat transfer and adsorption/desorption simulations with increasing levels of complexity.

Modeling efforts have focused on the validation and calibration of high fidelity CFD models through comparison with experimental data from NETL's Carbon Capture Unit (C2U) The following bubbling fluidized bed cases have been investigated: AX cold flow, 32D cold-flow, 32D hot non-reacting flow, and 32D reacting flow.

Figure 16 illustrates the experiment setup for AX cold flow and 32D flow. Experiments for AX and 32D shared the same basic configuration, but more quantity of interest (QOI) measurements have been collected for 32D, especially for the reacting flow.

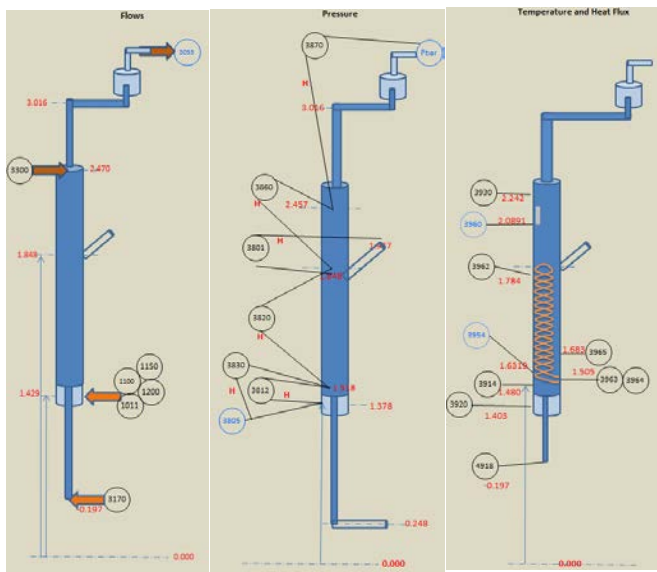

(a) **(b)** **(c)**

Figure 16: Illustration of Experiment Setup for AX and 32D Flow

<u>Multiphase CFD Modeling of AX Cold Flow in C2U Batch Unit</u>. Simulation results for the 2D axisymmetric MFIX model for the AX cold flow in a batch unit have been completed. A total of 120 cases of this simulation with 6 UQ parameters have been run and the result data post-processed and provided to the UQ team. Figure 17 shows the comparison of simulation results and the experiment measurements. Two apparent discrepancies can be observed:

1. While the experiment data show pressure drop PDT3820 decreases with increasing flow rate, CFD predictions with constant particle size of 115μm (Sauter mean diameter) do not show such trend.
2. The predicted pressure drops are higher than the experimental values, particularly at higher flow rates.

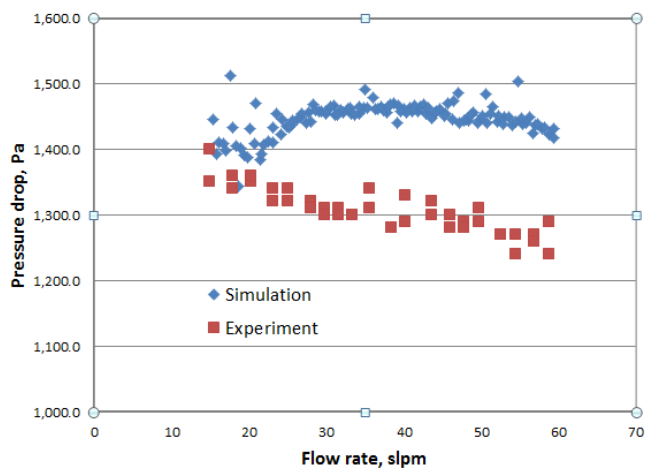

Figure 17: Pressure Drop PDT3820 vs. Flow Rate

Additional AX cold flow simulations were then carried out to identify the source of the discrepancies mentioned above. Since the sorbent particle size follows a distribution, with some particles smaller than SMD and some larger than SMD, simulations with bi-modal particle sizes were next performed to study the effect of particle size on pressure drop in the fluidized bed. Results in Figure 18 indicate that simulations with two particle sizes with a bi-modal distribution generate the desired trend of pressure drop vs. flow rate, but the MFIX simulation with a bi-modal particle size requires about three times the Central Processing Unit (CPU) time for a single particle size.

The above results indicate that an effective particle size, not SDM, must be used to accurately capture the hydrodynamics of the fluidized bed should a single particle size be required due to computational constraints. This finding led us to add the particle size as an additional calibration parameter. Subsequently, a total of 60 refined cases with 6 UQ parameters have been run and the result data post-processed and provided to the UQ team. Figure 19 shows the comparison of simulation results with C2U experimental measurements. A similar trend of pressure drop vs. flow rate is observed in this new batch of simulations.

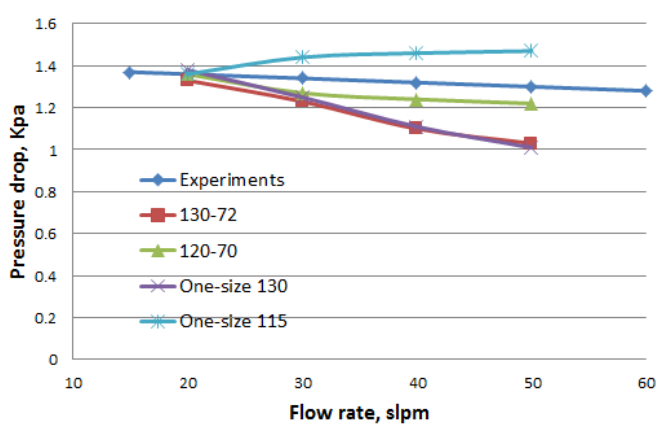

Figure 18: Pressure Drop PDT3820 vs. Flow Rate, with Different Particle Sizes

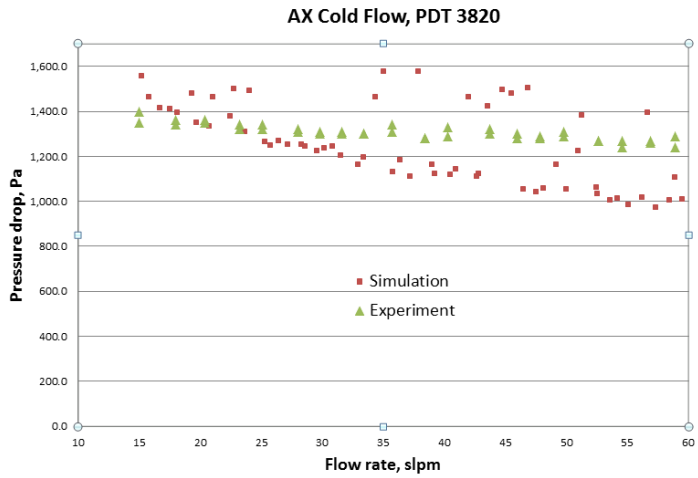

Figure 19: Pressure Drop PDT3820 vs. Flow Rate, with 7 UQ Parameters Including Particle Size

In summary, the sorbent particle size plays a significant role on pressure drop, and its calibration is crucial in achieving the high fidelity CFD simulation results on the hydrodynamics of the fluidized bed. Similar particle size effect will be discussed in the following 32D cold flow, hot non-reacting flow, and the reacting flow.

Multiphase CFD Modeling of 32D Cold and Hot Non-reacting Flow in C2U Batch Unit. The model setup is similar to what has been developed for AX cold flow, as described above, but replacing the particle properties with those of 32D, including particle size, density and total mass. Coils act as no slip BCs for hydrodynamics and heating boundaries for thermal kinetics. All temperature setting information were extracted from the experiment data and input into the MFIX model accordingly. In the experiment, the temperatures were measured by thermal couples TE3962A and TE3965, and their time averaged values are used as a QOI for validation and calibration. In the C2U experiment, the pressure drops were measured by pressure transducer PDT3820 for cold flow, and by both PDT3820 and PDT3860 for hot flow. Eight sets of experimental data were selected, covering the whole range of flow rates (15- 60 slpm) and temperatures (40-800 ºC). The steady state of hydrodynamics is reached after 100s; however, the thermal kinetics reaches its steady state after 700s. The validation of steady-state temperatures in different cases is summarized in Figure 20, while pressure drop over the whole reactor height is shown in Figure 21. Two different particle sizes are considered to address the effect of particle size on hydrodynamics. Three findings are summarized as below:

1. Simulation results show good agreement with the experimental data;
2. Particle size has a significant effect on pressure drop, and due to its uncertainty in experimental measurements, a calibration procedure including particle size is essential in our high fidelity CFD validation;
3. The thermal boundary condition imposed on coils accurately captures the thermal kinetics.

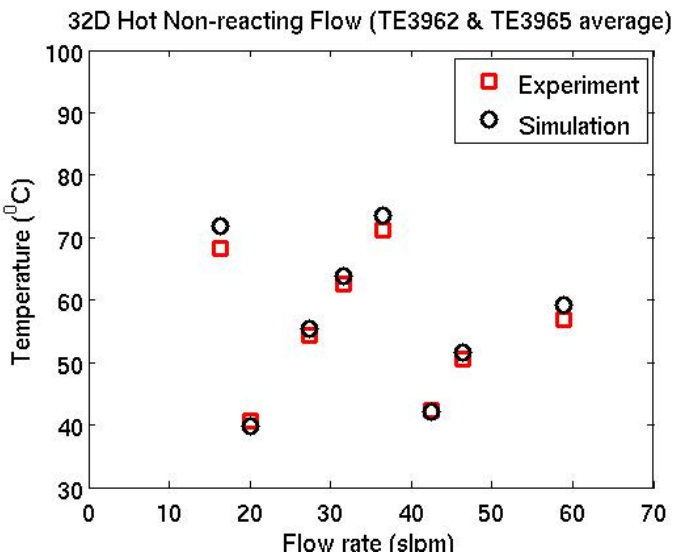

Figure 20: Validation of Steady-State Temperature in 32D Hot Non-Reacting Flow.

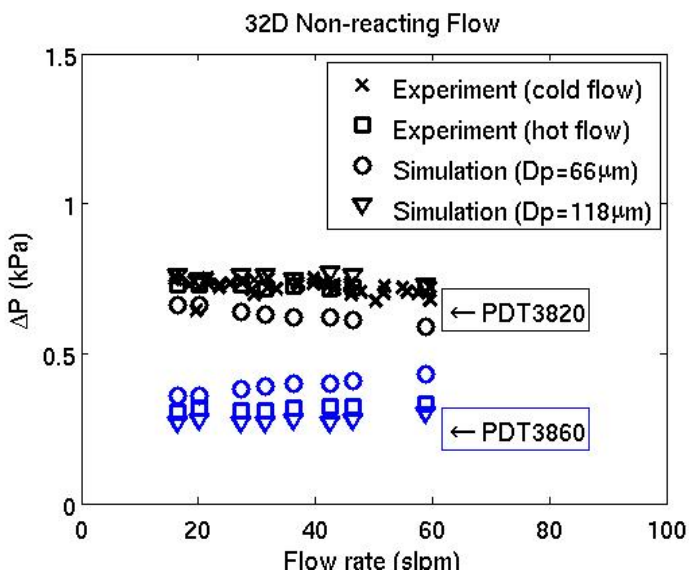

Figure 21: Validation of Pressure Drop in 32D Cold Flow and Hot Non-Reacting Flow.

The effect of transient boundary conditions were also studied using MFIX simulations. A series of 32D hot, non-reacting batch runs with transient boundary conditions was carried out. The gas inlet temperature, gas inlet flow rate and coil temperature all vary with time according to the recorded experimental data. The predicted temperature transients in the bed follow the experimental data closely, within a couple of degrees accuracy, at three locations in the bed (below coils, mid bed and top of the bed), as illustrated in Figure 22 to Figure 24.

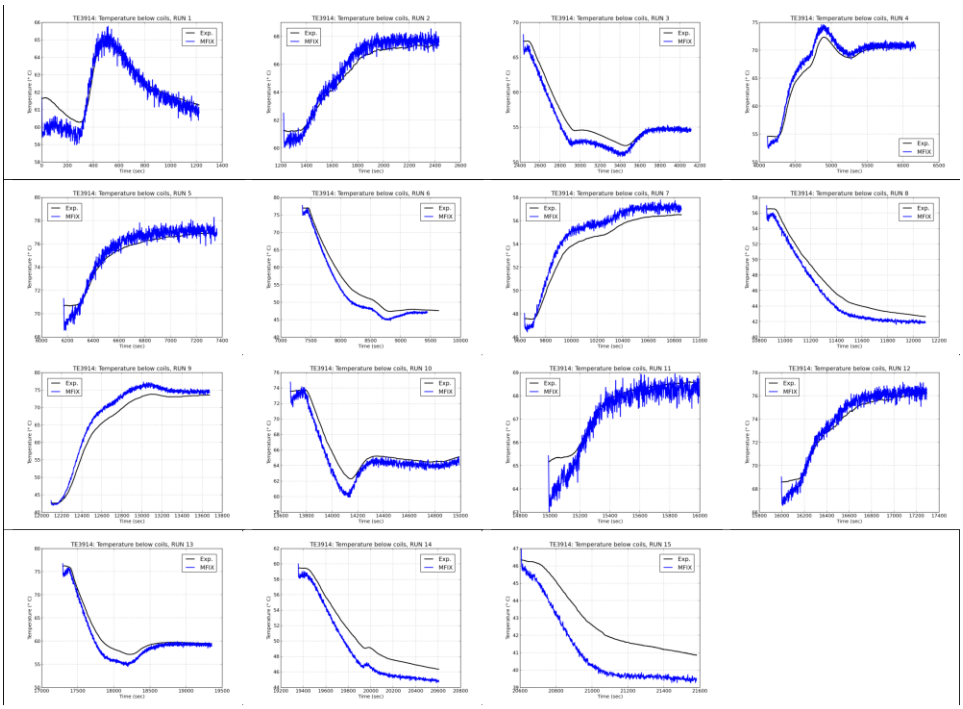

Figure 22: Bed Temperature Below Coils, for First 15 Flow Conditions.

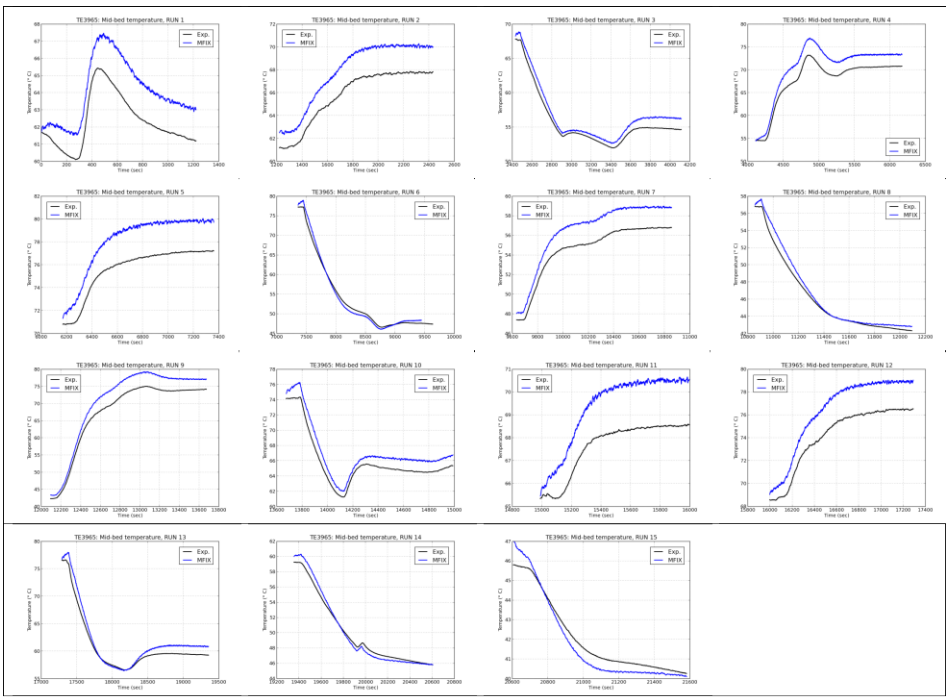

Figure 23: Bed Temperature at Mid-Bed Location, for First 15 Flow Conditions.

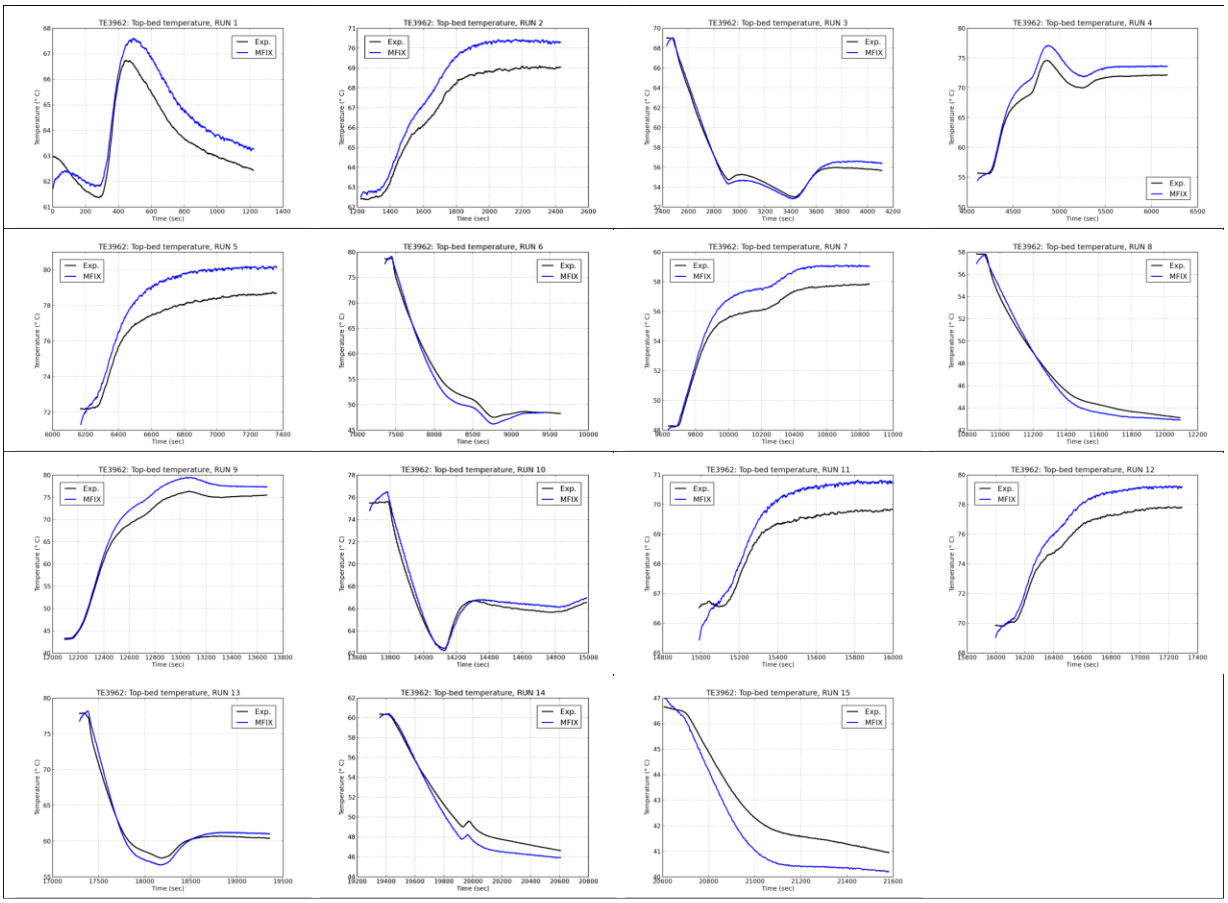

Figure 24: Bed Temperature at Top Of Bed, for First 15 Flow Conditions.

<u>UQ Tool for CFD & Hierarchical Validation Methodology</u> The general Bayesian calibration and model assessment methodology using a Bayesian BSS-ANOVA emulator (i.e., reduced model) was developed into a computational tool. The BSS-ANOVA-UQ tool takes as input experimental results in the form of input settings and resulting output(s), along with simulation results in the form of parameter and input settings and resulting output(s). It then performs a Bayesian calibration to find a posterior distribution of parameter settings for the simulator that allows it to best reproduce the experimental data. There is also a model form discrepancy function that is estimated in the calibration to allow for the fact that for reasonable parameter settings it is not always possible for the simulations to perfectly mimic reality. Implicit in the calibration routine is an emulator to allow the procedure to explore the parameter space at locations where the simulator was not evaluated. The emulator is a fast statistical approximation of the simulator that admits uncertainty about its predictions of what the simulator would say at untried locations.

The tool release includes with two detailed example use cases:

1. The literature based bubbling fluidized bed example. Here there are two correlated outputs.
2. The cold flow case of the C2U with AX sorbent. Here there is one output that is a time series of values once in steady state.

This tool has been also been used to calibrate the C2U cold flow case with AX that was re-run in order to allow the “effective” particle size to be a calibration parameter. In principle the particle size distribution is

known, but only one value can be specified in MFIX due to computational time constraints. The realization that we made was that the effective particle size to use should be close to the Sauter Mean Diameter, but not necessarily equal to it. The resulting posterior distribution for the AX cold flow case is provided in Figure 25. The posterior distributions are shown as histograms of the MCMC sample along with the assumed prior distributions (blue curves). None of the model parameters (except particle size) exhibited significant changes from the prior, indicating pressure drop is not sensitive to any of these other model parameters. The SMD is approximately 115 microns, and the most appropriate size to use in MFIX is 117 micron (with very little variability). The MFIX output pressure drop is very insensitive to the other five parameters involved in the calibration, within their respective ranges.

We have also calibrated the same C2U cold flow case with the 32D sorbent (including particle size as a parameter). In this case there is a bimodal distribution of the 32D particles. That is, there is really a mixture of two component distributions. Therefore, the SMD should be calculated for each of the components, and in principle two particle sizes could be used in MFIX. However, after some pilot runs it was clear that using one particle size near SMD of the larger component distribution was sufficient. The calibrated posterior distributions are provided in Figure 20. We are in the process of performing a similar calibration, including sorbent kinetics parameters, using C2U reactive case data.

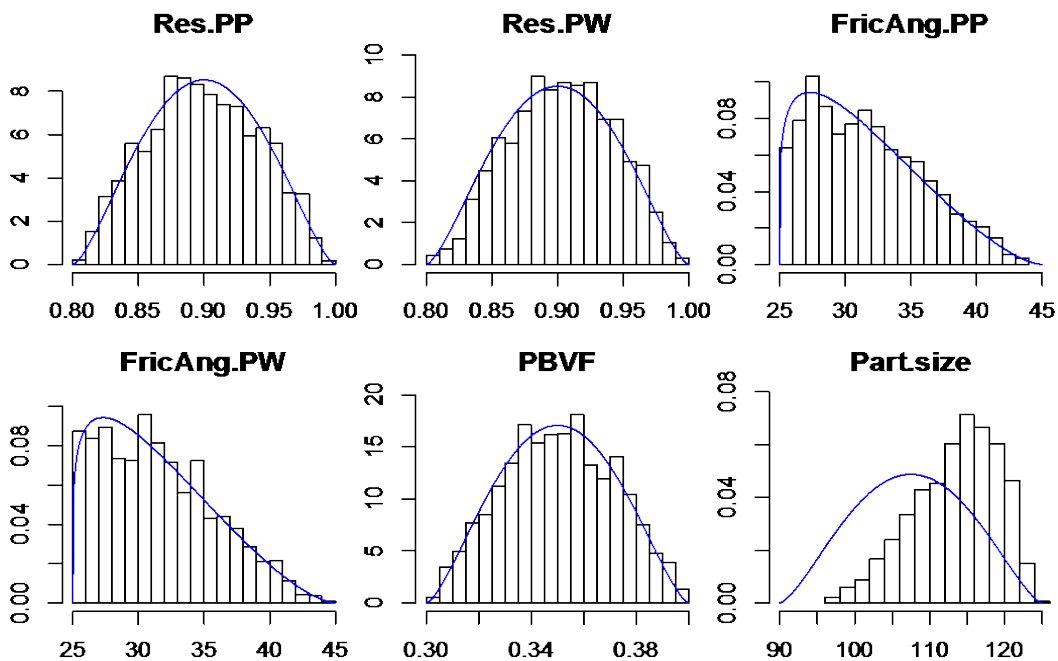

Figure 25: Marginal Posterior Distributions of the Six Model Parameters for MFIX

<u>Development of an Advanced UQ Methodology for CFD Models</u>. Full scale CFD models of multi-phase reactive flow simulations for CCSI applications may take several days to even weeks to run, making brute force parametric studies infeasible when reaction kinetics and heat transfer are included in the model-simulations. Therefore, it is important to develop time efficient surrogate models derived from a finite number of simulations. We developed a novel Bayesian treed multivariate Gaussian process (BTMGP) to model the uncertainty of multivariate simulation experiments, which can also handle discontinuities and localized features. In addition, we developed sequential sampling techniques to sequentially sample multivariate output in the most informative input with the help of the proposed BTMGP and expert prior

knowledge. In a Bayesian formulation, prior distribution of the computer experiment output is updated in light of the new observation and is conditional on various hyper-parameters. We utilize this model to sequentially sample the input space for the most informative values, taking into account model uncertainty and expertise gained. The simultaneous BTMGP fitting and sequential adaptive sampling gives a better prediction fit than other well known RMs.

Development of REVEAL Framework for RMs and Data Management. The REVEAL framework now automatically generates RM for multi-species MFIX model, by building in support for appropriate conversions between species mass fractions and individual mass flow rates at each inlet and outlet ports. MFIX models provide species data in form of mass fractions. When sampling mass fraction, the sum of the mass fractions must equal 1 to enforce constraints on the material balances.

To provide users the maximum flexibility with sampling of species data while conforming to composition requirements, REVEAL converts species mass fractions to individual mass flow rates and makes them available to users for sampling. The flow rates can be sampled independently of each other and are converted back to species mass fractions by normalizing with total flow rate. REVEAL then automatically performs conversions to generate appropriate MFIX input files (with mass fraction data) and runs the MFIX models. The data gathered can be analyzed using the integrated graphical tools for sensitivity and error analysis. The tool was also extended to supports the export of multi-species MFIX model data for ACM or CAPE OPEN simulations.

We also extended the REVEAL framework for working with any generic data server, setup on any Linux system. REVEAL uses a data server to support user level data management, data provenance, data sharing across multiple users as well as data persistence over multiple sessions. Prior to this release, it came pre-configured with a data server setup at PNNL. We generalize the data server setup process, provide REVEAL server side installers, a server set up guide and generalize the server configuration options in the REVEAL client. This will allow REVEAL users to work with any data server. This is important for deployment of this toolset component to industry so that they can directly control access to any proprietary data.

Work has also begun on the design and development of REVEAL-lite, a standalone toolset to create RMs with CFD results enabling its incorporation in process simulations. REVEAL-lite will run on a Windows host and will not require any other system to function. REVEAL-lite will facilitate automated creation of simulation input files and RM creation given the simulation sampled and output data. The RM can be created as a CAPE OPEN compliant module or as an ACM model file. The system will have support for Barracuda and MFIX CFD models.

Task 5.0 Process Models

This task includes the development of steady state and dynamic process models necessary for process synthesis, design, and simulation. Specific models developed during FY13 include a (1) bubbling fluidized bed reactor model, (2) moving bed reactor model, (3) CO_2 compression system model, (4) baseline MEA model, and (5) high viscosity solvent model.

Bubbling Fluidized Bed (BFB) model. A number of BFB models with different configurations were completed as shown in Figure 26. For each configuration, a converged model is part of the upcoming toolset release. Users can test the model by running the existing model or can provide their inputs.

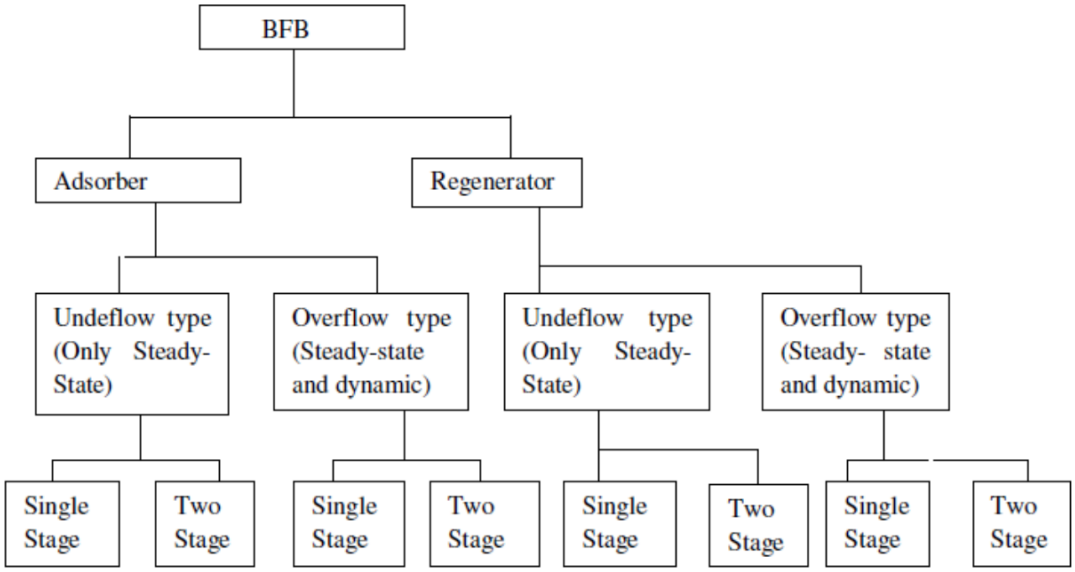

Figure 26: BFB Model Configurations.

A number of plots were developed to show the profile of the key transport variables. Figure 27 shows the concentration profiles of CO_2 and H_2O for the underflow type configuration. Figure 28 shows the temperature profiles of the lower stage in two-stage underflow type configuration, and Figure 29 shows the transients in CO_2 capture under open loop condition due to 10% step change in the flue gas flowrate.

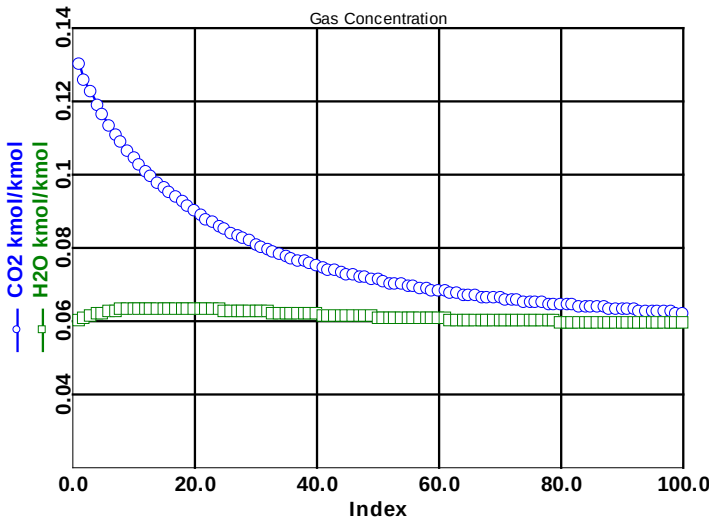

Figure 27: Gas Concentration Profile Plot for Underflow Type Configuration.

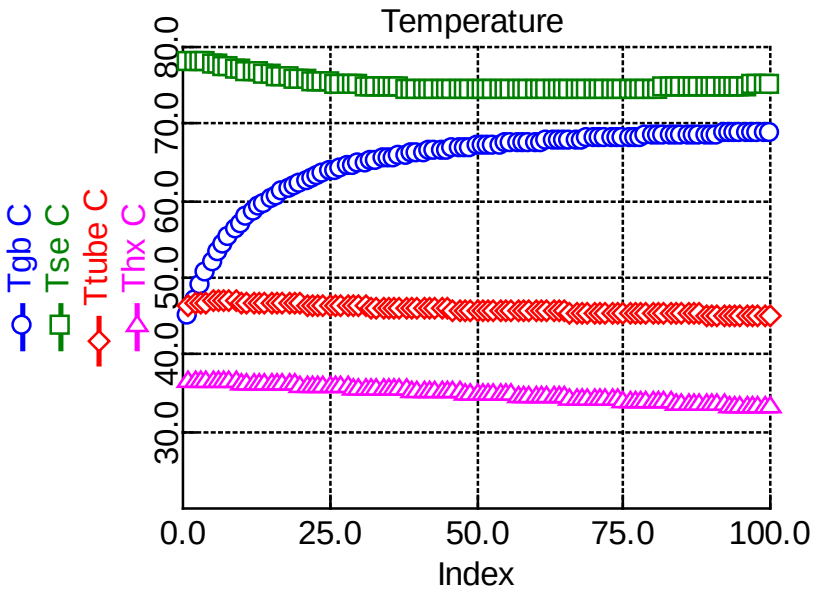

Figure 28: Temperature Profile Plot of Lower Stage Adsorber in 2-stage Underflow Type Configuration.

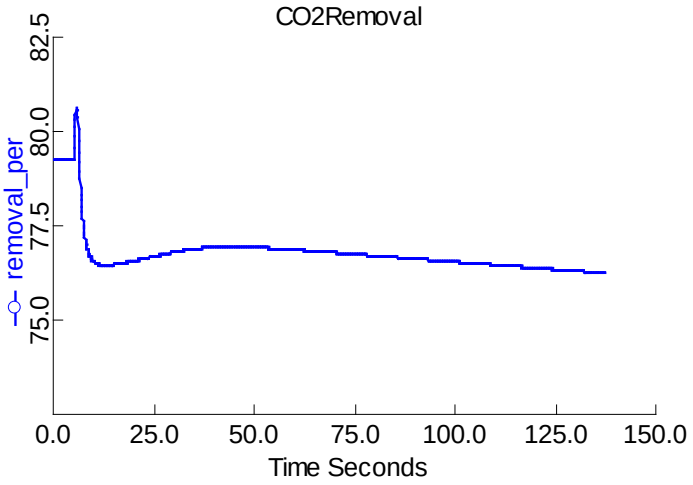

Figure 29: Dynamics of Overall CO_2 Capture for a Disturbance of 10% Step Change in Flue Gas Flowrate.

The BFB models can also be used to simulate the regenerator. Figure 30 shows the temperature profile for the overflow-type configuration, and Figure 31 shows the temperature profile in the lower stage of a two-stage regenerator with underflow-type configuration.

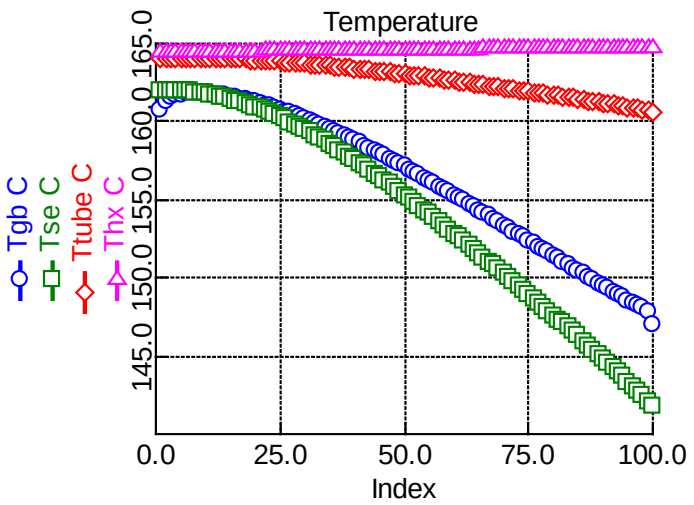

Figure 30: Temperature Profile Plot for Overflow Type Configuration.

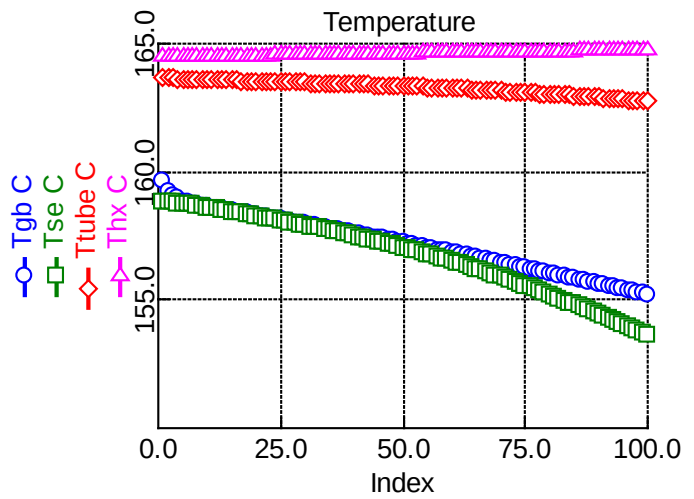

Figure 31: Temperature Profile Plot of Lower Stage Regenerator in 2-stage Underflow Type Configuration.

Moving bed model. The updated moving bed model has been completed and includes dynamic simulation capability. The features of the updated model are:

- External mass transfer resistance has been taken into account while calculating the surface concentration of reactants/products
- Heat exchanger model has been modified by considering packet-renewal theory
- Pre- and post-heat exchangers have been integrated within the bed
- Mass transfer and reaction kinetics were also modeled in addition to heat transfer in both pre- and post-heat exchangers.
- Solids temperature at any location in the bed is less than 130°C.

The pre- and post-heat exchangers integrated with the regenerator are used for heat recovery from the hot solid sorbent leaving the bed. Additional steam is used in the bed for heating. The inlet conditions of tube side fluid are designed such that the solids temperature at any location in the bed does not exceed 130°C which is the maximum operating temperature for avoiding material degradation. The heat transfer coefficients between the heat exchanging medium and the solid sorbent/ gas are modeled by using the packet-renewal theory. This theory results in a higher accuracy of the heat transfer coefficients. The profiles of solids temperature and solids loading are shown in Figure 32 and Figure 33, respectively.

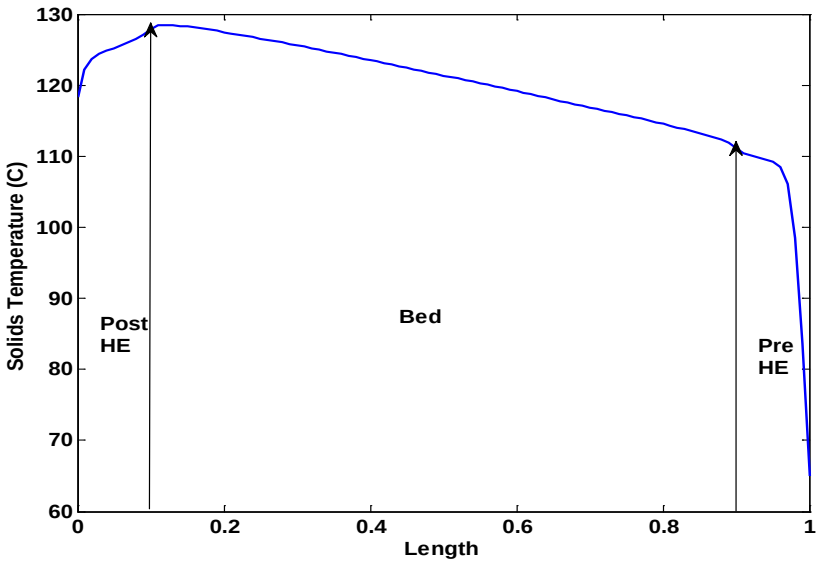

Figure 32: Solids temperature profile in the regenerator

A steep increase in the solids temperature at the top of the bed (right side boundary) is due to the pre-heat exchanger design and high driving force. A drop in the solids temperature at the bottom of the bed (left side boundary) is mainly due to the post heat exchanger. It can be noted that while it is possible to design the pre-heat exchanger for slow rise in temperature, undesired adsorption of water takes place below certain temperature as shown in Figure 33.

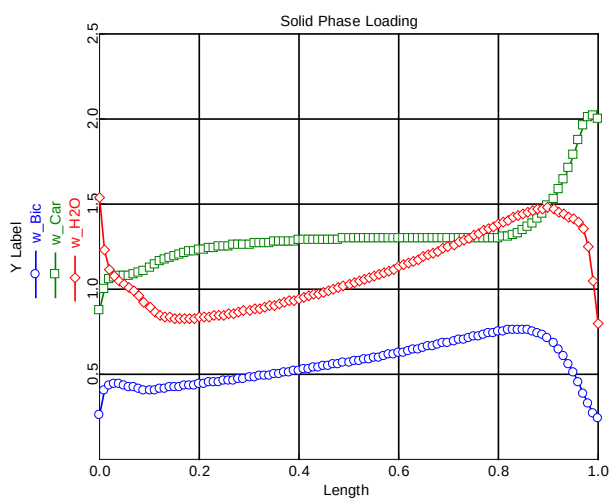

Figure 33: Molar loading of the ions in the regenerator

Figure 33 shows that in both the pre- and post-heat exchangers, the forward reaction i.e. adsorption takes place for both H_2O and bicarbonate. The rate of adsorption is significant for water in the post heat exchanger due to presence of steam. Adsorption rate of bicarbonate is very small. These phenomena were not observed in the earlier model, as the mass transfer/reactions were neglected in pre- and post-heat exchangers. This would be expected due to low temperature of the solids based on the current kinetics.

The results of the updated MB model are compared with the previous MB and current BFB models under similar inlet conditions and stream locations. With the decreased inlet temperature in all the models, the solids temperature profiles for all the models are shown in Figure 34. The solids temperatures are almost similar in the bed. A steep increase in the solids temperatures are observed in the case of MB. A drop in the solids temperature at the bottom of the bed (left side boundary) in the current MB model is mainly due to the post-heat exchanger in the latest MB model. The solids exit conditions from all the models are shown in Table 4.

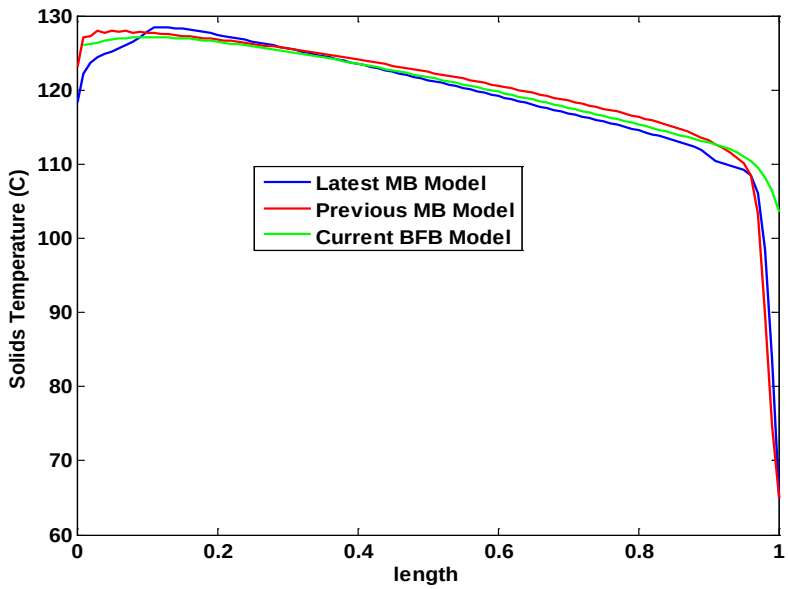

Figure 34: Comparison of solids temperature profiles in all the models

Table 4: Solids exit conditions from the bed

Species (mol/kg solid)	Current MB model with pre and post HE	Previous MB model	Current Bubbling fluidized bed model
Carbamate	0.874677	0.903943	0.902894
Bicarbonate	0.258409	0.267146	0.366067
Water	1.53518	1.22684	1.05588

Figure 35 shows the transient response in the solids loading as the inlet steam flowrate to the bed is increased. An increase in the steam flowrate results in an overall increase in the partial pressure of steam in the bed and as a result bicarbonate and carbamate loading decreases, but loading of physisorbed water increases.

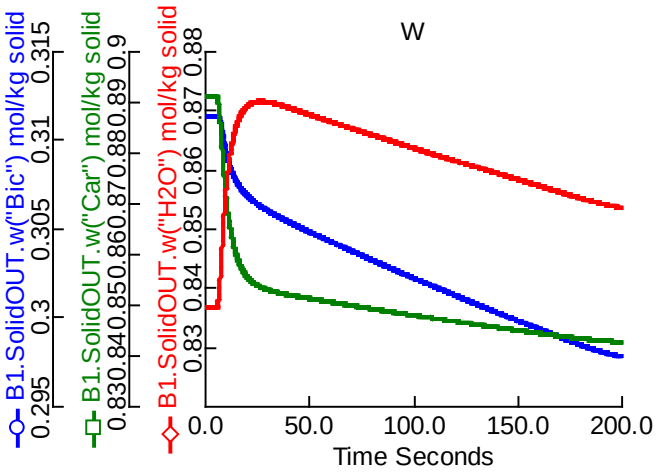

Figure 35: Transients in Solids Loading as a Result of a Ramp Increase in the Steam Flowrate to the Regenerator.

<u>Model of the Steam-BFW System</u>. The pressure-driven steam/boiler feed water (BFW) model shown in Figure 36 was developed to enable dynamic modeling of a potential heat recovery system for a solid sorbent system. A pressure network was developed between pre- and post- heat exchangers along with level and temperature controllers. During plant operation, the amount of steam condensed in the pre-heat exchanger may not match with the amount of BFW required in the post-heat exchanger. Hence, inlet and outlet control valves have been designed to supply the additional BFW for removal of excess water, respectively.

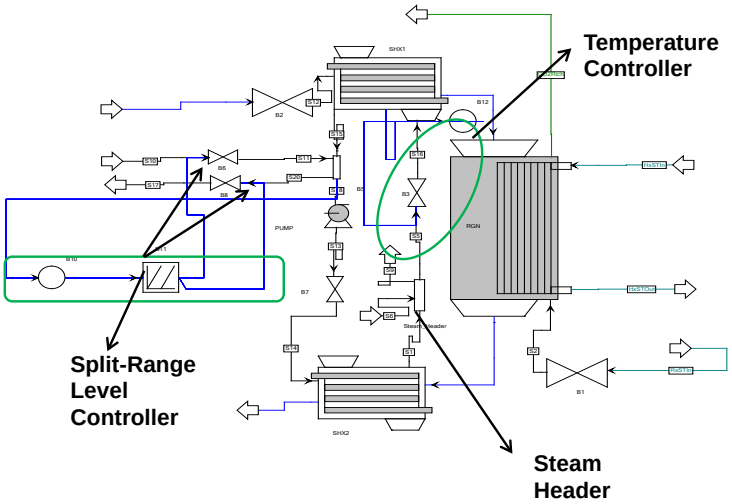

Figure 36: ACM Flowsheet of the Moving Bed Regenerator along with the Steam/BFW System.

A split range controller has been designed for manipulating both the inlet and outlet valves to maintain the required level. In addition, a control valve and a level controller have been designed to maintain the required water level in the post heat exchanger by manipulating the flow of BFW.

Model of the Pneumatic Transport System: Models of the pneumatic transport system for transporting solids from the adsorber to the regenerator and from the regenerator to the adsorber were developed. The transport medium was determined by comparing the power required by various options four possible mediums were considered. These mediums are the flue gas at the inlet of the adsorber, clean flue gas from the outlet of the adsorber, a recycling transport medium with makeup from the clean gas, and CO_2 from the outlet of the regenerator. If a portion of the inlet flue gas that enters the adsorber is considered for solids transport, a minimum of 8% and 7% of the total flue gas would be needed for transporting the solids from the adsorber to the regenerator and for transporting the solids from the regenerator to the adsorber, respectively. This means that flue gas used for transport must be recycled to the adsorber to achieve the overall target of 90% CO_2 capture. If a portion of the clean flue gas from the outlet of the adsorber is used, it should be compressed for transportation. The compression power is less in this case in comparison to the inlet flue gas as the molecular weight of the clean flue gas is lower and the flow required in both the cases is similar. The third option that has been considered is a recycling transport gas. In this case, the transport gas is separated from the solid sorbent in the feed hopper at the end of transport and then compressed, cooled, and recycled back again for transportation. When a recycling transport medium is considered, the advantage is that compression power is required only to compensate for the pressure drop in the lift pipe. Considering the clean gas as the recycling transport medium, the recycling option was found to be the optimal option. When CO_2 from the outlet of the regenerator was considered, a higher compression cost was required mainly due to its higher molecular weight. Therefore, the final pneumatic model was developed by considering the recycling option.

CO_2 Compression System Model. The steady-state models of both integral-gear and in-line compressors developed in FY12 have been extended to dynamic models. In addition, a pressure-driven model of the entire compression system with an eight stage compression system integrated with inter-stage coolers, flash vessels and a TEG water absorption system was developed. Commercial performance curves were used to develop a generalized set of coefficients that enable off-design characteristics to be predicted for compressors operating under a wide range of conditions. The resulting model includes a surge detection algorithm. In addition, a gain-scheduling controller has been developed for surge control.

AspenPlus MEA Solvent System Model. The model of the pilot plant at UT, Austin has been completed and used to simulate the operating conditions for which experimental data are available. In addition, a preliminary model of the National Carbon Capture Center (NCCC) solvent pilot plant has been developed. These models will be validated following a planned MEA campaign in the NCCC in March of 2014.

AspenPlus High Viscosity Solvent System Model. Thermodynamic and kinetic models for 8 m 2MPZ have been developed and validated with experimental data and a preliminary system model was completed and documented. In addition, a preliminary model for predicting heat exchanger area as a function of viscosity and pressure drop was developed in Aspen Plus and incorporated into an Aspen Plus® HEATX block in the heat transfer coefficient subroutine.

Task 6.0 Process Optimization & UQ

This task focuses on developing and demonstrating optimization and UQ tools that can be used to design and optimize an entire process, while concurrently quantifying the error associated with model predictions. These tools fall into three major categories: (1) development of algebraic surrogate models that can be used in a superstructure formulation, (2) a framework for the direct optimization and UQ of complex simulations, and (3) an alternative equation-based framework for oxycombustion process synthesis.

Algebraic Surrogate Model Builder for Optimization. The primary accomplishment of our efforts in this context is the development of the ALAMO code for the Automated Learning of Algebraic Models for Optimization, which allows detailed process, such as those developed under Task 5, to be used within rigorous, derivative-based optimization codes. These codes enable the optimization algorithms to determine optimal process configurations.

A considerable amount of effort was put in the development of a Fortran implementation of ALAMO. While developing this implementation, memory- and CPU-efficient data structures were invented that facilitate the application of ALAMO to industrial-scale problems. In addition progress was made on the development of a web interface for ALAMO in order to facilitate end-user applications of ALAMO.

ALAMO builds a surrogate using a best subset technique that leverages an integer programming formulation to allow for the efficient consideration of a large number of possible functional components in the model. The model is then improved systematically through the use of derivative-free optimization solvers to adaptively sample new simulation or experimental points. Comparing ALAMO and a variety of machine learning techniques, including simple least squares regression, and the lasso, ALAMO provides simpler models. Figure 37 shows the difference between the number of terms in the model provided by the three different modeling techniques and the number of terms in the simulated systems used for the comparison. An ideal modeling technique would result in zero or negative differences. As seen in this graph, the models obtained by the lasso are simpler than those obtained by least squares, while the models obtained by ALAMO are even simpler.

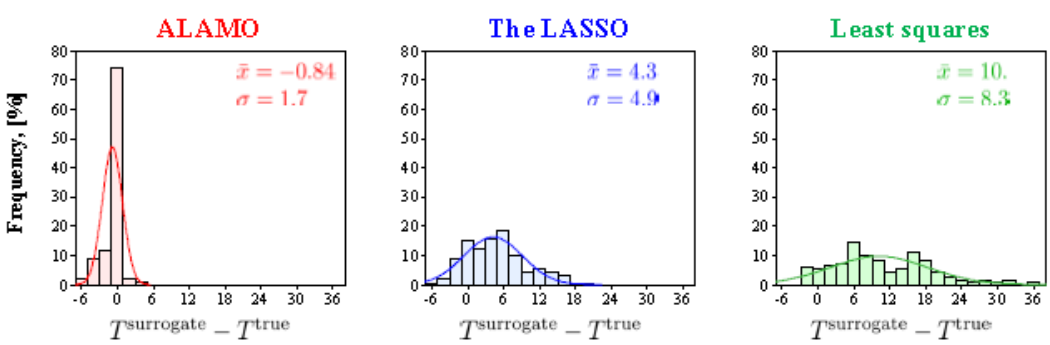

Figure 37: Comparison of Different Surrogate Modeling Techniques

Framework for Optimization and Quantification of Uncertainty and Sensitivity (FOQUS). The FOQUS tool combines the capabilities of the simulation based optimization framework and the uncertainty quantification framework into a single workflow and user interface. The tool connects to a simulation gateway (Task 9) for running large-scale parallel simulations.

The optimization component of the framework is based on a meta-flowsheet, which provides connectivity between process models. Each model potentially uses different modeling software, and recycle streams are often present. Improvements have been made to the optimization framework to better handle finding and solving tear streams in the meta-flowsheet. The framework has also been updated to run all simulations through the Turbine Gateway, and improvements have been made that increase the number of simulations, which can be run in parallel while using Turbine with optimization and UQ methods.

A generic system for connecting derivative free optimization (DFO) solvers for simulation-based optimization has been developed. Depending on the solver and the implementation, some solvers may be more parallelizable than others. Currently CMA-ES (https://www.lri.fr/~hansen/) is fully implemented while others are in early development and have been partially tested. A goal for the near future is to implement a wider variety of solvers, and begin work on optimization under uncertainty.

A heat integration module has been developed and integrated with the optimization capability to obtain the best performance of the process, as shown in Figure 38. Within each iteration of optimization, the process simulator takes process inputs (including initial inputs and intermediate results from the optimizer), performs function evaluations, and returns production information, such as raw material consumption rates, production rates and equipment sizes, to the optimizer; the heat integration tool receives information about process streams, such as flow rates and temperatures, from the results of the process simulator, and calculates the minimum utility consumption and number of heat exchangers; the optimizer minimizes the total cost, which is calculated from results of the process simulator and heat integration, and optimizes decision variables (part of simulation inputs) by derivative-free optimization methods. The heat integration tool is based on the transshipment model.

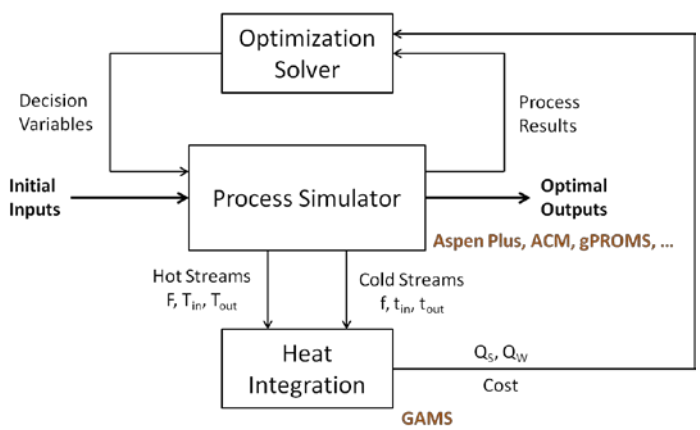

Figure 38 Simulation based optimization framework with heat integration

To demonstrate the importance of incorporating heat integration when optimizing a carbon capture process, a example case was run utilizing the CCSI base case solid sorbent process. When heat integrating with the steam cycle, the net efficiency of the power plant (with capture) was increased from 35.1% to 37.1%.

The first version of the Windows-based UQ GUI includes four categories of UQ capabilities. The first is a suite of computational tools for parameter screening, the purpose of which is to down-select the potentially large set of uncertain parameters via low-cost qualitative screening. The second category comprises a suite of methods for analyzing uncertainties and sensitivities (first, second, or total order), a screen shot of which is given below. Again, the first step is to select which set of runs to analyze from the top part of the screen. In addition to displaying the uncertainty and sensitivity results, there are also

options to visualize the sample data. The third category consists of methods for generating, validating, and visualizing response surfaces (or surrogates) given a sample (with inputs and model outputs); as well as uncertainty and sensitivity analysis based on the validated response surface. A number of response surface types are available from the underlying UQ computational engine. The validated response surface can then be analyzed for output uncertainties and parameter sensitivities. The fourth category comprises inverse UQ methods, that is, to recover true input parameter uncertainties given observations (with uncertainties) on the output. This inversion process is performed using Bayesian analysis with the Markov Chain Monte Carlo algorithms.

<u>GAMS modular oxycombustion optimization framework</u>. An ASU superstructure enables to optimizer to consider many different ASU configuration, resulting in optimization of both the ASU connectivity and operating conditions. The superstructure (Figure 39) allows for vapor and or liquid to be feed to the top, a middle and/or the bottom tray of the distillation column. Using the superstructure, an ASU design without a top condenser was selected; the nitrogen rich recycle from the high pressure column is instead used to provide reflux, a common configuration for many ASU systems.

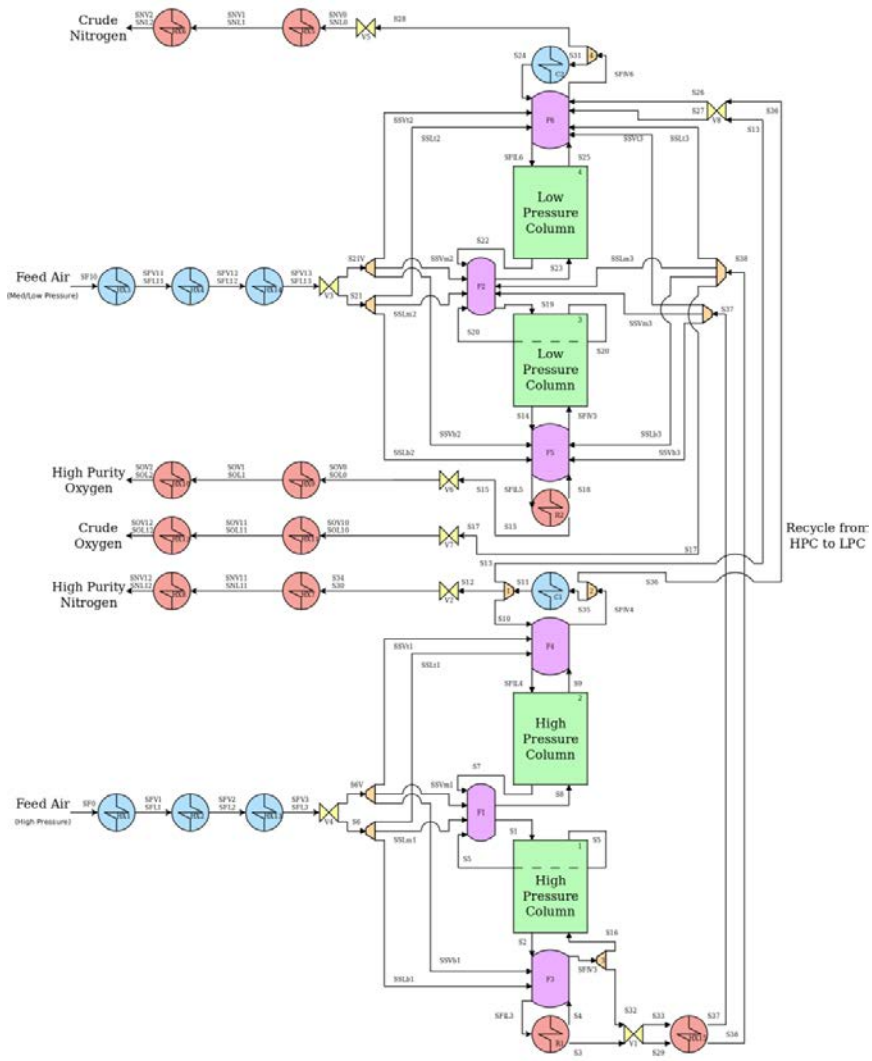

Figure 39: ASU Superstructure.

The thermodynamics module was extended to support any general cubic equation state. It was originally restricted to the SRK model. In addition binary interaction parameters from literature were added for the SRK and PR models as defaults to the framework.

A new model for distillation optimization was developed. The new model maintains the rigorous of tray-by-tray models while avoiding integer variables – greatly improving optimizer performance. This is done by adding bypass streams to each tray in the standard Mass, Equilibrium, Summation and Heat (MESH) equation model. The new model, coupled with the custom multistart initialization algorithm, was used to identify ASU designs competitive with other DOE reports.

The ASU results obtained with GAMS were validated against Aspen Plus simulations. This was done by simulating the second reboiler in Aspen Plus. The reboiler feed conditions and outlet vapor fraction are set to match the GAMS results. Agreement between the two programs in excellent, as shown below in the table and figure (Figure 40).

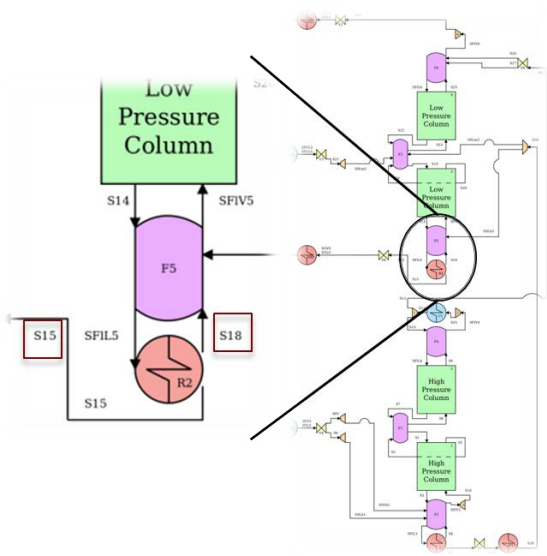

Stream	Prop	GAMS	Aspen
S18 (vapor)	N_2	11.03%	11.05%
	O_2	86.33%	86.31%
	Ar	2.64%	2.64%
S15 (liquid)	N_2	3.07%	3.09%
	O_2	**95.00%**	**94.96%**
	Ar	1.93%	1.95%
	Temp.	89.42 K	89.39 K

Figure 40: Comparison of GAMS and AspenPlus Results for Reboiler 2.

The best ASU results obtained with the superstructure, MESH with bypass model and multistart initialization procedure were compared with literature. The GAMS optimized specific energy is 0.174 kWh/kg of O_2 (assuming 86% eff. compression, ΔT_{min} = 1.25K) for 95% purity O_2. This corresponds very well with the specific energy of 0.179 kWh/kg O_2 reported in Cost and Performance for Low-Rank Pulverized Coal Oxycombustion Energy Plants by the DOE (2010). The DOE reported ASU specific energy is an estimate from a vendor after some optimization.

The framework includes optimal design of the multistream heat exchanger, which enables easy future extension to consider heat integration between the ASU and other parts of the power plant (such as the CO_2 processing unit). This capability is unique to the framework. Most other studies consider the ASU as a black-box provided by a vendor, which prevents integration strategies from being fully studied.

Task 7.0 Integrated Framework for Dynamics & Control

The primary focus of this task is the development and application of new, advanced process control techniques, that address specific dynamic operational challenges associated with integrating CO_2 capture and compression systems with coal fired power plants. Dynamic reduced models (D-RMs) enable faster computation of system responses enabling the development of an advanced process control framework and the integration of the dynamic models within a larger dynamic simulation. Two D-RM approaches are being pursued: data-driven D-RMs and reduced-order D-RMs.

Data-driven D-RMs use pre-computed results from repeated simulations of high-fidelity dynamic models over a range of input/output variable values and are suitable for offline dynamic simulations, as well as real-time simulations and online control applications due to the short CPU time required. However, data-driven D-RMs generally have limited accuracy and are valid only in the operating conditions that are sampled during the D-RM generation process. D-RM Builder is utilizing the data-driven approach.

Reduced-order D-RMs are more rigorous and developed from the underlying differential and algebraic equations in the high-fidelity models. Reduced state space models are not as fast as data-driven D-RMs in term of CPU time required but are valid over a wider range of operating conditions and are suitable for offline dynamic simulations and, in some cases, model-based real-time applications, such as advanced process control.

Dynamic Reduced Model Builder (D-RM Builder). D-RM Builder is a new software tool for automatic generation of data-driven D-RMs. It includes the Decoupled AB Network (DABNet) model for multiple-input-multiple-output (MIMO) systems. The original research paper (Sentoni et al., 1998) on the DABNet model was for multiple-input-single-output (MISO) systems. For a system with multiple outputs, we generate multiple DABNet models, one for each output variable. The advantage of this approach is that we can use different pole values and system matrices (A and B matrices) for different outputs in case the time constants for different output variables with respect to input variables are quite different. In other words, this approach is very flexible to model a complicated system with some output variables that respond very quickly while others very slowly, thereby leading to an accurate D-RM. One disadvantage is that multiple system matrices and neural networks need to be calculated and trained, respectively, during the D-RM building stage and used during the prediction stage. D-RM Builder also includes the nonlinear autoregressive moving average (NARMA) model as an alternative data-driven D-RM model.

To handle cases where the high-fidelity dynamic models may be difficult to converge, the D-RM Builder user can use ramp changes to replace step changes of input variables for the simulations. Due to the stiffness of the differential equations inherent in a hard-to-solve model, a large step change could cause the solver to fail. However, small step changes that mimic a ramp change can be used to approximate a large step change and avoid the solver failure. The revised D-RM Builder allows the user to turn on this option and specify the ramp rate for an input variable that is susceptible to the solver failure.

D-RMs generated by D-RM Builder are in MATLAB script format. To use them for dynamic simulation or for model predictive control, three MATLAB classes were developed to work with the exported D-RMs. The MATLAB class files are packed as a part of D-RM Builder installation. An example driver code in MATLAB was also developed that can run the script file of a generated D-RM and construct a D-RM object based on the type of D-RM (DABNet or NARMA) and the variables assigned in the D-RM file. The member functions of the MATLAB D-RM classes were developed to initialize the input, output, and state variables and to update them one step at a time to simulate a dynamic process. The driver code is also included in the D-RM Builder installation.

Reduced-Order D-RMs. Spatially distributed first-principle dynamic process models give an accurate physical description of chemical processes, but lead to large-scale models whose numerical solution is challenging and computationally expensive. Thus, fast dynamic reduced-order models (ROM) are required for model-based real-time applications, such as advanced process control.

In this work, we have developed a computationally efficient and accurate dynamic ROM for a BFB adsorber. The ROM is generated by a quasi-steady state approximation for the fast states. An eigenvalue analysis technique is utilized to locate fast and slow dynamic modes and a spectral association method is applied to associate states with eigenvalues. From Figure 41, we can see a clear separation of two distinct eigenvalue groups in the original system. By analyzing the unit perturbation spectral resolution (UPSR) matrix, the ten eigenvalues in the fast mode are associated with nine gas phase mass balance states in all three regions and one gas phase energy balance state in the emulsion region, which are converted to algebraic equations in the ROM. By comparing the curves shown in Figure 41, we can tell that, in the reduced-order system, all the eigenvalues in fast mode are removed, which proves our eigenvalue-to-state association correct.

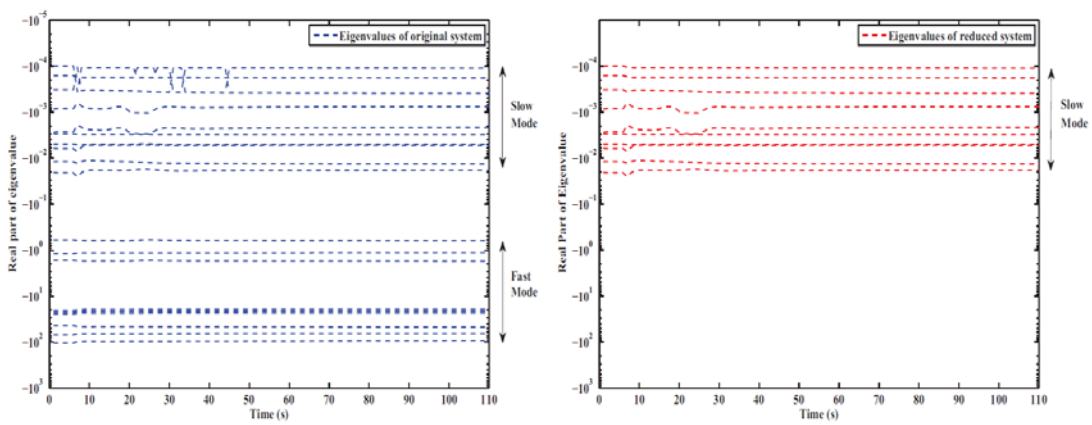

Figure 41: Eigenvalue Variation during the Transient Response of the Full and Reduced System.

Neglecting the axial variations in temperature and pressure, the time scale decomposition result of the single tray model is applied to the full BFB model. After removing the fast states, half of the differential equations are converted into algebraic equations. A case study is conducted to validate the ROM, in which a ±25% step change in the flue gas flow rate is introduced at t=0s and t=200s, respectively. The CO_2 capture fraction and sorbent loading are key outputs, which indicate the efficiency of the adsorber. The dynamic behavior of these two outputs predicted by both the reduced-order and the full BFB model have nearly the same dynamic behavior. The detailed simulation data are listed in Table 5. The computational cost is reduced by 33.02% in the ROM.

Table 5: Simulation Results, 1-CO_2 Removal Fraction, 2-Sorbent Loading

	Simulation time(s)	MRE1	MSE1	MRE2	MSE2
Full model	427	-	-	-	-

ROM	286	7.2%	2.98E-6	1.2%	2.02E-6

Based on simulation test and physical analysis, we can conclude that the ROM generated by eigenvalue analysis and time scale decomposition can greatly reduce the computational cost with very small errors in predicting the model's key outputs. Moreover, this systematic approach could also be applied to other systems apart from the BFB adsorber.

Advanced Process Control (APC) Framework. Significant progress was made towards development of an APC framework based on data-driven D-RMs. Constrained dynamic-matrix-control (DMC) was developed corresponding to the transition function (input-to-state mapping) within the DABNet D-RMs based on Laguerre networks for controlling Laguerre states (i.e., assumed observable). In addition, the neural-network mapping portion of the D-RM, alongside the transition function, was used as a 'control-model' to predict and control measured outputs. With the nonlinear prediction methodology in place for both the transition and observation function, an unconstrained "black-box" nonlinear model predictive controller (NMPC) was coded with rate of input change and deviation from set point included within the cost-function. The control algorithm was implemented and tested on a BFB D-RM as the 'real-plant' and a less accurate D-RM, generated by significantly less training data, as a 'control-model'. The control responses were very promising compared to linear model predictive control (MPC) using linear models obtained directly using MATLAB's System Identification Toolbox.

Task 8.0 Risk Analysis & Decision Making

This task focuses on the development of tools to assess risk based on the state of technology development, technical risk associated with a given design, and financial risk. The major accomplishment was the development of an initial version of the technical risk model and the development of prototype technology readiness level (TRL) tools.

TRL-based risk tools. The TRL tools include (1) a TRL likelihood model (TRL-LM), which is a wiki-based expert elicitation system to compile information and estimate the likelihood (probability) that each technology/process has matured through each maturity level, (2) a TRL-uncertainty model (TRL-UM), which estimates (based on previous industry experience) the "true" uncertainty for a given simulation based on the current TRL level. A beta version of the current TRL model has been developed. This model enhances the capabilities of the likelihood model (TRL-LM) and implements our uncertainty modeling methodology (TRL-UM). A fully functional, tested, and documented version is expected to be completed in January 2014.

Technical Risk Model. A spreadsheet for Technical Risk was completed. Commercialization of new CCSI technology will include two key elements of risk management, namely, technical risk (will the process and plant performance be effective, safe, and reliable?) and enterprise risk (can project losses and costs be controlled within the constraints of market demand to maintain profitability and investor confidence?). Both of these elements of risk are incorporated into our risk analysis products. A prototype Technical Risk Model (TRM) has been developed that quantifies risk and system reliability based on the expected equipment component mechanical and electrical/control failure rates and mean down times (MDT) for a theoretical carbon capture system retrofitted to a 650 $MW_{electric}$ pulverized coal electric power generator.

Microsoft Excel has been used to assemble the technical risk model input data and calculate initial system reliability information based on discrete values for component failure rates and MDTs. This segment of the TRM is called the Technical Risk Input for Carbon Capture Simulation (TRICCS) workbook. A sample session of this workbook is shown in Figure 42.

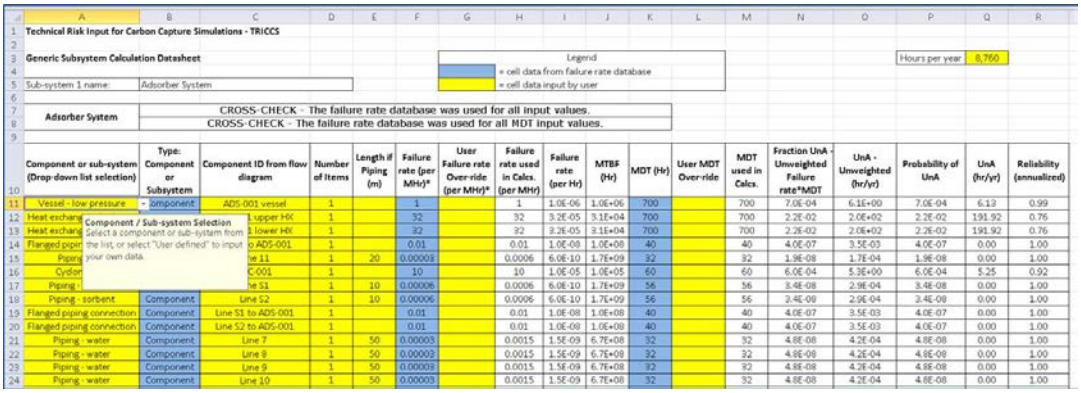

Technical Risk Input for Carbon Capture Simulations - TRICCS

Generic Subsystem Calculation Datasheet

Legend: = cell data from failure rate database; = cell data input by user

Hours per year: 8,760

Sub-system 1 name: Adsorber System

Adsorber System: CROSS-CHECK - The failure rate database was used for all input values. CROSS-CHECK - The failure rate database was used for all MDT input values.

Component / Sub-system Selection: Select a component or sub-system from the list, or select "User defined" to input your own data.

Component or sub-system (Drop down list selection)	Type: Component or Subsystem	Component ID from flow diagram	Number of Items	Length if Piping (m)	Failure rate (per MHr)*	User Failure rate Over-ride (per MHr)*	Failure rate used in Calcs. (per MHr)	Failure rate (per Hr)	MTBF (Hr)	MDT (Hr)	User MDT Over-ride	MDT used in Calcs.	Fraction UnA - Unweighted Failure rate*MDT	UnA - Unweighted (hr/yr)	Probability of UnA	UnA (hr/yr)	Reliability (annualized)
Vessel - low pressure	Component	ADS-001 vessel	1		1		1	1.0E-06	1.0E+06	700		700	7.0E-04	6.1E+00	7.0E-04	6.12	0.99
Heat exchang		upper HX	1		32		32	3.2E-05	3.1E+04	700		700	2.2E-02	2.0E+02	2.2E-02	191.92	0.76
Heat exchang		lower HX	1		32		32	3.2E-05	3.1E+04	700		700	2.2E-02	2.0E+02	2.2E-02	191.92	0.76
Flanged pipin		o ADS-001	1		0.01		0.01	1.0E-08	1.0E+08	40		40	4.0E-07	3.5E-03	4.0E-07	0.00	1.00
Piping		e 11	1	20	0.00003		0.0006	6.0E-10	1.7E+09	32		32	1.9E-08	1.7E-04	1.9E-08	0.00	1.00
Cyclon		C-001	1		10		10	1.0E-05	1.0E+05	60		60	6.0E-04	5.3E+00	6.0E-04	5.25	0.92
Piping -		e S1	1	10	0.00006		0.0006	6.0E-10	1.7E+09	56		56	3.4E-08	2.9E-04	3.4E-08	0.00	1.00
Piping - sorbent	Component	Line S2	1	10	0.00006		0.0006	6.0E-10	1.7E+09	56		56	3.4E-08	2.9E-04	3.4E-08	0.00	1.00
Flanged piping connection	Component	Line S1 to ADS-001	1		0.01		0.01	1.0E-08	1.0E+08	40		40	4.0E-07	3.5E-03	4.0E-07	0.00	1.00
Flanged piping connection	Component	Line S2 to ADS-001	1		0.01		0.01	1.0E-08	1.0E+08	40		40	4.0E-07	3.5E-03	4.0E-07	0.00	1.00
Piping - water	Component	Line 7	1	50	0.00003		0.0015	1.5E-09	6.7E+08	32		32	4.8E-08	4.2E-04	4.8E-08	0.00	1.00
Piping - water	Component	Line 8	1	50	0.00003		0.0015	1.5E-09	6.7E+08	32		32	4.8E-08	4.2E-04	4.8E-08	0.00	1.00
Piping - water	Component	Line 9	1	50	0.00003		0.0015	1.5E-09	6.7E+08	32		32	4.8E-08	4.2E-04	4.8E-08	0.00	1.00
Piping - water	Component	Line 10	1	50	0.00003		0.0015	1.5E-09	6.7E+08	32		32	4.8E-08	4.2E-04	4.8E-08	0.00	1.00

Figure 42: Example Screen Shot from the Input System Worksheet of TRICCS.

The prototype TRICCS workbook is based on the selection of specific system design components and technical factors believed to be important determinants of the expected performance of the carbon capture system, subject to uncertainty. The uncertainty surrounding the selected technical performance variables is propagated in a model that calculates the expected failure rate, system unavailability, and system reliability for each of the sub-systems and the total carbon capture system. The model measures risk in terms of the contributions to system reliability of various components and sub-systems. The results are presented in both tabular and graphical formats. Results of an initial (example) analysis are shown in Figure 43.

	Failure rate (per MHr)	Failure rate (per Hr)	MTBF (Hr)	MDT (Hr)	Probability of UnA	UnA (hr/yr)	Reliability (annualized)
Adsorber System	580	5.80E-04	1,724	104	0.057	499	6.21E-03
CO2 Prep System	197	1.97E-04	5,076	40	0.008	68	1.78E-01
Flue Gas Prep System	711	7.11E-04	1,406	124	0.081	712	1.97E-03
Regenerator System	2,394	2.39E-03	418	67	0.138	1,209	7.80E-10
Sorbent Transport System	460	4.60E-04	2,174	59	0.026	231	1.78E-02
Total System	**4,342**	**4.34E-03**	**230**	**79**	**0.256**	**2,242**	**3.02E-17**

Component count summary by system	Blowers	Compressors	Controllers	Cyclones	Flanges	Heat Exchangers	Moving Beds	Piping (m)	Pumps	Solids Conveyance	Valves	Vessels	User Defined
Adsorber System	0	0	4	1	3	2	0	240	1	0	7	1	0
CO2 Prep System	0	0	2	0	1	1	0	200	1	0	3	0	0
Flue Gas Prep System	0	1	2	0	1	1	0	175	1	0	5	0	0
Regenerator System	1	1	13	0	0	3	0	390	1	0	14	1	0
Sorbent Transport System	0	0	2	0	4	0	0	50	0	2	0	0	0
Totals	**1**	**2**	**23**	**1**	**9**	**7**	**0**	**1,055**	**4**	**2**	**29**	**2**	**0**

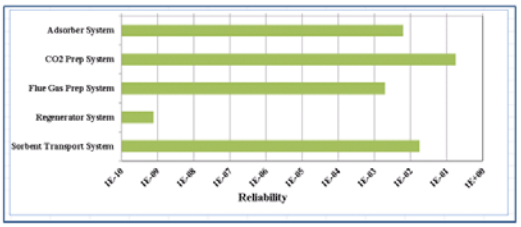

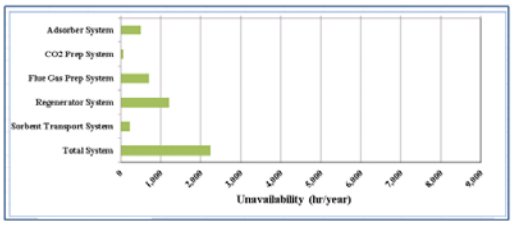

Figure 43: Example Screen Shots from the Summary & Aggregation Worksheet of TRICCS.

The TRICCS workbook is designed to allow flexible definition of systems and subsystems, while tying them to real-world component identification and failure rate data. Part of the flexibility provided allows the user to insert plant-specific component failure rate and repair time data in place of the built-in data. After gaining experience using the TRICCS workbook, multiple instances of this workbook can be used to develop subsystem data that can then be used in place of components to build a more complicated system model.

Task 9.0 Crosscutting Integration Tools

Data Management System. A comprehensive technology survey resulted in identifying Alfresco as the preferred data storage engine for the data management framework. It supports rich web client access, numerous file system access methods, and methods for programs to interact with the system. In addition, it is supported by both a large open source community and a commercial entity. For programs that do not already have a data format for their large-scale data, HDF5 is the recommended file format for data storage. For configuration files, we recommend adopting JSON.

Turbine Science Gateway. This server and gateway architecture enables remote execution of a series of simulations to enable parameter sweeps and a series of simulations in support of optimization and uncertainty quantification. The gateway supports execution on cloud compute resources, clusters and local machines. An "Excel" web application was added to Turbine to enable the running of the optimization team use-case, where a spreadsheet is run after each set of simulation runs to perform a variety of additional calculations. Support for gPROMS simulations was also added to complement the previous support for Aspen Plus and Aspen Custom Modeler.

In order to support the use case where the user does not have ready access to an Amazon Cloud Service, a simpler Turbine Science Gateway installer "TurbineClusterGateway" was developed for installing the gateway on single machines or on clusters. This installer lacks all Amazon Web Services specific functionality and simplifies installation.

Product Deployment. This task focused on preparing for and packaging the upcoming release of the CCSI Toolset. This release will provide major functionality to industry users and has many significant tools that are being released. Managing the release process, particularly extensive testing, is a critical aspect of CCSI. Because the tools being developed among the various tasks are intended for use by industry, it is essential that each component of the CCSI Toolset can be accessed, installed and utilized as intended. A continuous build and integration system was developed, which provides automated nightly builds of the software products in the CCSI Toolset. This will ultimately enable continuous integration and testing of code to ensure that issues introduced by new code are recognized quickly.

3.0 Conclusion

During FY13, CCSI announced the initial release of its first set of computational tools and models during the October 2012 meeting of its Industry Advisory Board. This initial release led to five companies licensing the CCSI Toolset under a Test and Evaluation Agreement this year. By the end of FY13, the CCSI Technical Team had completed development of an updated suite of computational tools and models, which includes 12 new products and significant updates to 11 products from the previous release to provide new capabilities and improved usability. The new tools include an integrated Framework for Optimization and Quantification of Uncertainty and Sensitivity (FOQUS), a validated CFD model to predict particle attrition, and a new tool to create RMs of dynamic simulations to enable more effective study of the operational characteristics of potential carbon capture systems. Another new tool enables the use of advanced Bayesian statistical methods for calibration and validation of models. Finally, a new basic data submodel for a high-viscosity carbon capture solvent was developed following CCSI's recent expansion into this area.

The goals for CCSI are to continue the development of the computational tools, models, methodologies and infrastructure that will ultimately become the CCSI Toolset. This development will proceed in parallel with the demonstration of these tools for specific capture technologies. The demonstrations will highlight the new capabilities that the CCSI Toolset will ultimately provide for facilitating the scale up and commercialization of new carbon capture technology. Additional releases of the CCSI Toolset are planned for Fall 2014 and Fall 2015, with a final release in January 2016.

4.0 Technology Transfer

Agarwal, K., Sharma, P., Ma, J., Lo, C., Gorton, I., and Yan, L., “REVEAL: An Extensible Reduced Order Model Builder for Simulation and Modeling,” *Computing in Science and Engineering*, April 11, 2013. IEEE computer Society Digital Library. IEEE Computer Society, http://doi.ieeecomputersociety.org/10.1109/MCSE.2013.46

Agrawal, K., Holloway, W., Milioli, C., Milioli, F., and Sundaresan, S., “Industrial Application of Computational and Numeric Approaches to Particle Flow II,” presented at the 2012 AIChE Annual Meeting, Pittsburgh, PA, October 28 - November 2, 2012.

Agrawal, K., Holloway, W., Milioli, C., Milioli, F., and Sundaresan, S., “Filtered Models for Scalar Transport in Gas-Particle Flows,” published in *Chemical Engineering Science*, 95, May 24, 2013, p. 291-300.

Bhattacharyya, D., and Miller, D.C., “US Department of Energy's Carbon Capture Simulation Initiative: Computational Tools for Accelerating Process Development,” presented at the PSE:APM Forum 2013, New York, NY, June 5-6, 2013.

Carney, J. E., Sun, X., and Sundaresan, S., "Report on CFD Modeling for Solvent Absorption and Preliminary Strategy for Developing High Resolution Closure Models for Corresponding Large Scale CFD Simulations", prepared for U.S. Department of Energy National Energy Technology Laboratory, May, 2013

Chen, Y., Grossmann, I., and Miller, D., “Optimization and Heat Integration in Simulation Models,” presented at the 2013 CAPD Annual Review Meeting, Pittsburgh, PA, March 11-12, 2013.

Cozad, A., Sahinidis, N.V., and Miller, D.C., “Alamo: Automatic Learning of Algebraic Models for Optimization,” presented at the 2012 AIChE Annual Meeting, Pittsburgh, PA, October 28 - November 2, 2012.

Cozad, A., Sahinidis, N.V., and Miller, D.C., “Strengthened Regression Models through Response Variable Bounds,” presented at the 2013 Energy Systems Initiative Annual Meeting, Pittsburgh, PA, March 10, 2013.

Cozad, A., Sahinidis, N.V., and Miller, D.C., “Surrogate-Based Optimization of Simulated Energy Systems,” presented at the 2012 AIChE Annual Meeting, Pittsburgh, PA, October 28 - November 2, 2012.

Cozad, A., Sahinidis, N.V., Yuan, Z., and Miller, D.C., “Optimizing Simulations and Black-Boxes using a Surrogated-Based Approach,” presented at the 2013 Center for Advanced Process Decision-Making Annual Review Meeting, Pittsburgh, PA, March 11-12, 2013.

Cozad, Sahinidis, Miller. “Learning surrogate models for simulation-based optimization.” Submitted to AIChE Journal. Sept. 2013.

Dowling, A.W., “Equation Oriented Coal Oxycombustion Flowsheet Optimization,” presented at the 12th Annual Conference on Carbon Capture Utilization & Sequestration, Pittsburgh, PA, May 13-16, 2013.

Dowling, A.W., and Biegler, L.T., “Optimization-Based Process Synthesis for Sustainable Power Generation,” *Chemical Engineering Transactions*, 35, 2013, p. 1-12. DOI:10.3303/CET1335001

Dowling, A.W., Biegler, L.T., and Miller, D.C., “Coal Oxycombustion Flowsheet Optimization,” presented at the 2012 AIChE Annual Meeting, Pittsburgh, PA, October 28 - November 2, 2012.

Dowling, A.W., Biegler, L.T., and Miller, D.C., “Pressure Swing Adsorption: Design and Optimization for Pre-Combustion Carbon Capture,” presented at the 2012 AIChE Annual Meeting, Pittsburgh, PA, October 28 - November 2, 2012.

Engel D, A Dalton, C Dale, J Thompson, R Leclaire, B Edwards, and E Jones, “Development of a Risk-Based Comparison Methodology of Carbon Capture Technologies,” *Greenhouse Gases: Science and Technology*, submitted September 2013.

Engel, D.W., Dalton, A., Dale, C., and Jones, E., “Risk-Based Comparison of Carbon Capture Technologies,” 12th Annual Carbon Capture, Utilization & Sequestration Conference, Pittsburgh, PA, May 13-14, 2013.

Kim, H., Haranczyk, M., Epperly, T., Abouelnasr, M., Swisher, J.A., Jariwala, K., Mebane, D.S., Smit, B., Kress, J.D., and Miller, D.C., “Integrating the Carbon Capture Materials Database with the Process Simulation Tools of the Carbon Capture Simulation Initiative,” presented at the 2012 AIChE Annual Meeting, Pittsburgh, PA, October 28 - November 2, 2012.

Konomi, B., Karagiannis, G., and Lin, G., “On Bayesian Treed Multivariate Gaussian Process with Linear Model of Coregionalization,” submitted to *Journal of Computer Statistics and Data Analysis*, July 10, 2013.

Konomi, B., Karagiannis, G., Sarkar, A., Sun, X., and Lin, G., “Bayesian Treed Multivariate Gaussian Process with Adaptive Design: Application to a Carbon Capture Unit,” submitted for revision to *Technometrics*, July 10, 2013.

Lane, W.A., Storlie, C.B., Montgomery, C., and Ryan, E.M., “Numerical Modeling and Bayesian Calibration of a Bubbling Fluidized Bed with Immersed Horizontal Tubes,” presented at ASME 2013 Fluids Engineering Division Summer Meeting (FEDSM2013), Incline Village, NV, July 7-11, 2013.

Lane, WA; C. Storlie, C. Montgomery, E.M. Ryan. “Numerical modeling and Bayesian calibration of a bubbling fluidized bed with immersed horizontal tubes.” Powder Technology, under review (2013).

Lee, Anita S.; John C. Eslick, David C. Miller, John R. Kitchin, Comparisons of amine solvents for post-combustion CO_2 capture: A multi-objective analysis approach, International Journal of Greenhouse Gas Control, Volume 18, October 2013, Pages 68-74, ISSN 1750-5836, http://dx.doi.org/10.1016/j.ijggc.2013.06.020.

Ma, J., Montgomery, C.J., Agarwal, K., Sharma, P., Lang, Y-D., Huckaby, D.E., Zitney, S.E., Gorton, I., Agarwal, D.A., and Miller, D.C., “Enforcing Elemental Mass and Energy Balances for Reduced Order Models Generated from CFD Simulations,” presented at the 2012 AIChE Annual Meeting, Pittsburgh, PA, October 28 - November 2, 2012.

Mebane, D.S., “Multi-Scale Modeling with Generalized Dynamic Discrepancy,” presented at the 2013 SIAM Annual Meeting, San Diego, CA, July 12, 2013.

Mebane, D.S., Bhat, K.S., and Storlie, C.B., "Uncertainty Quantification in Multi-Scale Models of Chemical Processes," Presented at CECAM Psi-k Workshop on Multi-Scale Modeling, Cap Roig, Spain, September 10, 2013.

Mebane, D.S., Bhat, K.S., Kress, J.D., Fauth, D.J., Gray, M.L., Lee, A. and Miller, D.C., "Bayesian Calibration of Thermodynamic Models for the Uptake of CO_2 in Supported Amine Sorbents using Ab Initio Priors," Physical Chemistry Chemical Physics 15 (2013) 4355-4366.

Mebane, D.S., Bhat, K.S., Kress, J.D., Miller, D.C., Morinelly, J.E., and Eslick, J.C., “Bayesian Methods in Multiscale Modeling,” presented at the 2012 AIChE Annual Meeting, Pittsburgh, PA, October 28 - November 2, 2012.

Mebane, D.S., Bhat, K.S., Moore, L.M., Kress, J.D., Fauth, D.J., and Gray, M.L., "Amine-Based Solid Sorbent Modeling in the Department of Energy's Carbon Capture Simulation Initiative," presented at 2012 MRS Fall Meeting, Boston, MA, November 25-30, 2012.

Mebane, D.S., Storlie, C.B., Kress, J.D., Moore, L.M., Bhat, K.S., Fauth, D.J., and Gray, M.L., "The Importance of Transport Processes in Silica-Supported, Polyethyleneimine-Impregnated CO_2 Sorbents," presented at the 2012 AIChE Annual Meeting, Pittsburgh, PA, October 28 - November 2, 2012.

Milioli, C., Milioli, F., Holloway, W., Agrawal, K., and Sundaresan, S., "Constitute Model for the Fluid-Particle Drag Coefficient in Filtered Two-Fluid Models for Gas-Particle Flows," presented at the 2012 AIChE Annual Meeting, Pittsburgh, PA, October 28 - November 2, 2012.

Milioli, C., Milioli, F., Holloway, W., Agrawal, K., and Sundaresan, S., "Filtered Two-Fluid Models of Fluidized Gas-Particle Flows: New Constitutive Relations," article first published online May 22, 2013, DOI: 10.1002/aic.14130, *AIChE Journal*, 59, 9, September 2013, p. 3265-3275.

Miller DC. Syamlal M, Mebane D, Storlie C, Bhattacharyya D, Sahinidis NV, Agarwal D, Tong C, Zitney SE, Sarkar A, Sun X, Sundaresan S, Ryan E, Engel E, Dale C. "Carbon Capture Simulation Initiative: A Case Study in Multi-Scale Modeling and New Challenges," *Annual Review of Chemical and Bimolecular Engineering*, submitted September 2013.

Miller, D. C., N. V. Sahinidis, A. Cozad, A. Lee, H. Kim, J. Morinelly, J. Eslick, Z. Yuan, "Computational Tools for Accelerating Carbon Capture Process Development". In Proceedings of The 38th International Technical Conference on Clean Coal & Fuel Systems, Clearwater, FL, USA. June 2 - 6, 2013.

Miller, D., "Advanced Computational Tools to Accelerate Technology Development," presented at the 2013 CAPD Energy Systems Initiative Meeting, Pittsburgh, PA, March 10, 2013.

Miller, D.C., "The Role of Process Integration in CO_2 Capture for GHG Abatement," Proceedings, International Process Integration Jubilee Conference, Gothenburg, Sweden, March 18-20, 2013.

Miller, D.C., and Fisher, J.C., "Accelerating Technology Development: Post Combustion Capture Sorbents," presented at the 2013 NETL CO_2 Capture Technology Meeting, Pittsburgh, PA, July 9, 2013.

Modekurti, S., Bhattacharyya, D., and Zitney, S.E., "Dynamic Modeling and Control of a Solid-Sorbent CO_2 Capture Process with Two-Stage Bubbling Fluidized Bed Adsorber-Reactor," presented at the 2012 AIChE Annual Meeting, Pittsburgh, PA, October 28 - November 2, 2012.

Modekurti, S., Bhattacharyya, D., and Zitney, S.E., "Dynamic Modeling and Transient Analysis of a Solid-Sorbent Adsorber for CO_2 Capture," *Proc. of the 29th Annual International Pittsburgh Coal Conference*, Pittsburgh, PA, October 15-18 (2012).

Modekurti, S., Bhattacharyya, D., and Zitney, S.E., "Dynamic Modeling and Control Studies of a Two-Stage Bubbling Fluidized Bed Adsorber-Reactor for Solid–Sorbent CO_2 Capture," *Industrial & Engineering Chemistry Research*, 52, 30, 2013, 10250–10260. DOI: 10.1021/ie400852k

Morinelly, J.E., and Miller, D.C., "Post-Combustion Gas Permeation Carbon Capture System Models," presented at the 2012 AIChE Annual Meeting, Pittsburgh, PA, October 28 - November 2, 2012.

Ryan, E.M., Decroix, D., Breault, R., Xu, W., Huckaby, E.D., Saha, K., Dartevelle, S., and Sun, X., "Multi-Phase CFD Modeling of a Solid Sorbent Carbon Capture System," *Powder Technology*, 242, 2013, p. 117-134.

Ryan, E.M., Lane, W.A., Montgomery, C., Storlie, C., and Wendelberger, J., “Validation and Uncertainty Quantification of Large Scale CFD Models for Post Combustion Carbon Capture,” presented at the ASME Validation and Verification Symposium, Nevada, May, 22, 2013.

Sahinidis, N.V., Cozad, A., and Miller, D.C., “Derivative-Free Optimization Enhanced-Surrogate Model Development for Optimization,” presented at INFORMS 2012, Phoenix, AZ, October 14-17, 2012.

Sarkar, A; W Pan, DM Suh, D Huckaby, X Sun. Flow dynamics of sorbent particles in a moving fluidized bed regenerator of a carbon capture unit. Accepted in Powder Technology, 2013.

Sarkar, A., Sundaresan, S., and Xin, S., “A Sub-Grid Model for an Array of Immersed Cylinders in Coarse-Grid Multiphase Flow Simulations of a Carbon Capture Device,” presented at 2012 AIChE Annual Meeting, Pittsburgh, PA, October 28 - November 2, 2012.

Sarkar, X. Sun, S. Sundaresan. “Sub-grid drag models for horizontal cylinder arrays immersed in gas-particle multiphase flows.” *Chemical Engineering Science*, 104(2013)399–412. dx.doi.org/10.1016/j.ces.2013.08.050.

Sherman, B. and Rochelle, G.T., "Viscosity Effects in Amine Scrubbing with 8 m 2-Methylpiperazine," Presented at the 2nd Post Combustion Capture Conference, Bergen, Norway, September 18, 2013.

Storlile, C.B., “Calibration of Computational Models with Categorical Parameters and Correlated Outputs via Baysian Smoothing Spline ANOVA,” presented at the Quality and Productivity Research Conference (QPRC), Niskayuna, NY, June 7, 2013.

Storlie, C.B., Lane, W.A., and Ryan, E.M., “Calibration of Computational Models with Categorical Parameters and Correlated Outputs via Bayesian Smoothing Spline ANOVA,” submitted to the *Journal of the American Statistical Association* (in review), July 2013.

Sundaresan, S. “Coarse-Grained Models for Momentum, Energy and Species Transport in Gas-Particle Flows.” Plenary Lecture at Fluidization XIV, May 26-31, 2013; Noordwijkerhout, The Netherlands.

Xu, W., D. Decroix and X. Sun, “Mechanistic Based DEM Simulation of Particle Attrition in a Jet Cup”, *Powder Technology*, under review (2013).

Yang, L. and I.E. Grossmann, “Water Targeting Models for Simultaneous Flowsheet Optimization,” *Ind.Eng.Chem. Research* (2012).

Yuan, Z.H., Cozad, A., Sahinidis, N.V., and Miller, D.C., “Surrogate Model Based Optimal Synthesis of Solid Sorbent Carbon Capture Process,” presented at the 2012 AIChE Annual Meeting, Pittsburgh, PA, October 28 - November 2, 2012.

5.0 References

Amundsen TG, Lars E, and Elmer DA. Density and viscosity of monoethanolamine + water + carbon dioxide from (25 to 80) °C. J. Chem. Eng. Data. 2009;54:3096-3100.

Chen, X. Carbon Dioxide Thermodynamics, Kinetics, and Mass Transfer in Aqueous Piperazine Derivatives and Other Amines. The University of Texas at Austin. PhD Dissertation. 2011.

Plaza, J. M. " Modeling of Carbon Dioxide Absorption Using Aqueous Monoethanolamine, Piperazine and Promoted Potassium Carbonate," PhD Thesis, UT Austin, 2011.

Sentoni, G. B., J. P Guiver, H. Zhao and L. T. Biegler, "A State Space Approach to Nonlinear Process Modeling: Identification and Universality,"*AIChE J.*, 44, 10, p. 2229 (1998).

The National Energy Technology Laboratory (NETL) conducts cutting-edge energy research and technology development and analyzes energy systems and international energy issues for the U.S. Department of Energy. The NETL-Regional University Alliance (NETL-RUA) is an applied research collaboration that combines NETL's energy research expertise with the broad capabilities of five nationally recognized, regional universities: Carnegie Mellon University (CMU), The Pennsylvania State University (PSU), University of Pittsburgh (Pitt), Virginia Tech, and West Virginia University (WVU), and the engineering and construction expertise of an industry partner (URS). NETL-RUA leverages its expertise with current fossil energy sources to discover and develop sustainable energy systems of the future, introduce new technology, and boost economic development and national security.

Cynthia Powell
Director
Office of Research and Development
National Energy Technology Laboratory
U.S. Department of Energy

Timothy McNulty
Associate Vice-President for Government Relations
Carnegie Mellon University

Neil Sharkey
Interim Vice President for Research
The Pennsylvania State University

Mark Redfern
Vice Provost for Research
University of Pittsburgh

Robert Walters
Vice President for Research
Virginia Tech

Fred King
Vice President for Research and Economic Development
West Virginia University

Kevin Donovan
RES Program Manager
URS Corporation

CCSI Executive Committee

Jared Ciferno
Director
Strategic Center for Coal
Office of Coal and Power R&D
National Energy Technology Laboratory
U.S. Department of Energy

Susan Maley
Technology Manager for Crosscutting Research
Strategic Center for Coal
Office of Coal and Power R&D
National Energy Technology Laboratory
U.S. Department of Energy

Cynthia Powell
Director
Office of Research and Development
National Energy Technology Laboratory
U.S. Department of Energy

Regis Conrad
Director, Division of Crosscutting Research
Office of Fossil Energy
U.S. Department of Energy

Madhava Syamlal
Focus Area Lead
Office of Research and Development
National Energy Technology Laboratory

David Brown
Division Director
Computational Research Division
Lawrence Berkeley National Laboratory

Melissa Fox
Program Manager
Applied Energy Programs
Los Alamos National Laboratory

John Grosh
Deputy Associate Director
Computation Directorate
Lawrence Livermore National Laboratory

Richard M. Russell
Manager HPC for Energy Cluster
Fundamental & Computational Science Directorate
Pacific Northwest National Laboratory

Edward S. Rubin
Professor
Carnegie Mellon University

Sankaran Sundaresan
Professor
Princeton University